# Hepatic SEC16B regulates lipid homeostasis by coordinating VLDL secretion and lipid droplet expansion

Wei Lu[1], Zhiming Zhao[1], Donald Molina[2], Huaxun Fan[3], Ruicheng Shi[1], Ye Tian[1], Raja Gopoju[4], Tiantian Yang[1], Xinyuan Zhang[1], Yanqiao Zhang[4], Kai Zhang[3, 5], Jaume Amengual[2, 6], Bo Wang[1,5,6,7*]

[1] Department of Comparative Biosciences, College of Veterinary Medicine, University of Illinois Urbana-Champaign, Urbana, IL, USA

[2] Department of Food Science and Human Nutrition, University of Illinois Urbana-Champaign, Urbana, IL, USA

[3] Department of Biochemistry, School of Molecular & Cellular Biology, College of Liberal Arts & Sciences, University of Illinois Urbana-Champaign, Urbana, IL, USA

[4] Department of Internal Medicine, University of Arizona College of Medicine, Phoenix, Phoenix, AZ, USA

[5] Cancer Center at Illinois, University of Illinois Urbana-Champaign, Urbana, IL, USA

[6] Division of Nutritional Sciences, College of Agricultural, Consumer and Environmental Sciences, University of Illinois Urbana-Champaign, Urbana, IL, USA

[7] Department of Molecular & Integrative Physiology, School of Molecular & Cellular Biology, College of Liberal Arts & Sciences, University of Illinois Urbana-Champaign, Urbana, IL, USA

* Correspondence: Bo Wang, Ph.D. 3840 VMBSB, 2001 S Lincoln Ave. Urbana, IL, USA, 61802 bowang@illinois.edu, 217-300-8084

**Conflicts of interest:** The authors have declared that no conflict of interest exists.

**Abstract**

The liver plays a critical role in lipid homeostasis, where lipids are either secreted as very-low-density lipoproteins (VLDL) or stored in lipid droplets (LDs). However, the regulatory mechanisms governing these two interconnected processes remain poorly understood. Here, we demonstrate that SEC16B functions as a lipid-responsive regulator in the liver, promoting VLDL secretion and LD expansion to handle lipid flux and maintain lipid homeostasis. Genome-wide association studies have identified single-nucleotide polymorphisms in *SEC16B* to be highly associated with serum lipid levels in humans. Hepatic *Sec16b* deficiency decreases serum lipid levels by impairing VLDL secretion through mechanisms that are at least partially independent of microsomal triglyceride transfer protein (MTP)-mediated ApoB lipidation and COPII-mediated intracellular trafficking. SEC16B partially localizes at ER-LD contact sites and promotes LD expansion by facilitating the targeting of ER proteins to LDs. More importantly, suppression of *Sec16b* dramatically lowers serum lipid levels and reduces atherosclerotic lesion size in *Ldlr* null mice. These data reveal a mechanism that coordinates VLDL and LD metabolism and suggest SEC16B as a potential therapeutic target for atherosclerosis treatment.

**Keywords:** Atherosclerosis, VLDL, ApoB lipidation, lipid droplet expansion

## Introduction

Dysregulation of lipid homeostasis is known to cause various diseases, including atherosclerosis and fatty liver diseases (1-3). Atherosclerosis, a chronic inflammatory disease, is triggered by the subendothelial retention of cholesterol-rich, ApoB-containing lipoproteins within arterial walls. While elevated low-density lipoprotein cholesterol (LDL-C) is a well-established risk factor for atherosclerosis (4, 5), recent human genetic evidence also supports a causal role for elevated triglyceride-rich lipoproteins (TGRLs), such as very-low-density lipoprotein (VLDL), in atherogenesis (2, 6). Although drugs targeting VLDL metabolism are available for treating hyperlipidemia, a substantial side effect is the accumulation of lipids in hepatocytes as lipid droplets (LDs), leading to fatty liver diseases (7). Thus, a better understanding of the regulation of VLDL and LD metabolism could open new avenues for the safe treatment of atherosclerosis. The liver plays a pivotal role in maintaining systemic lipid homeostasis by regulating lipid de novo biosynthesis, lipid uptake from circulation derived from dietary sources or fatty acids (FAs) released from adipose tissue during fasting, and the subsequent delivery of lipids to peripheral tissues in the form of VLDL (8). During the early stages of VLDL biogenesis, lipids are incorporated to apolipoprotein B (ApoB) within the endoplasmic reticulum (ER) (9). This process, known as lipidation, is facilitated by the microsomal triacylglycerol transfer protein (MTP) (10). Following the initial ApoB lipidation, nascent VLDL undergoes additional bulk lipidation prior exiting the ER to fuse with cis-Golgi. Its exit from the ER is considered to be the rate-limiting step in VLDL secretion (11). Due to its larger size, the egress of VLDL from the ER does not follow the canonical coat protein complex II (COPII)-mediated protein secretory pathway. Instead, its intracellular trafficking relies on specialized transport machinery known as VLDL transport vesicles (VTVs), which require components of COPII machinery (12).

However, the precise mechanisms controlling the lipidation and transport of VLDL from the ER to Golgi have not been fully elucidated.

LDs are highly dynamic organelles that function as temporary lipid storage and act as a sink to alleviate cellular lipid stress under physiological conditions in the liver (13). An imbalance in the processes maintaining lipid homeostasis can result in LD formation, particularly when lipid influx or synthesis exceeds the liver's capacity to secrete them as VLDL. LD biogenesis is initiated by neutral lipid accumulation in the ER bilayer, leading to oil lens formation. The oil lens bud off and form nascent LDs (14), which expand through local triglyceride (TG) synthesis and/or fusion with other smaller LDs (15, 16). Furthermore, ER-LD contacts facilitate lipid and protein exchange between ER and LDs, thereby sustaining LD growth (17). While the origins of VLDL and LDs differ, they share a similar structure characterized by a hydrophobic core containing TGs and cholesterol esters, enclosed by a phospholipid monolayer. Previous studies have demonstrated a close interconnection between VLDL and LD metabolism. Impaired VLDL secretion leads to increased LD formation, whereas LDs serve as potential reservoirs of substrates for VLDL lipidation (9, 18, 19). However, the regulatory mechanisms governing the interplay between VLDL secretion and LD metabolism remain poorly understood.

In this study, we identify SEC16B as a regulator of both VLDL and LD metabolism. By analyzing genome-wide association study (GWAS) datasets, we discovered significant associations between single-nucleotide polymorphisms (SNPs) in *SEC16B* locus and plasma cholesterol levels in humans. Both whole-body and liver-specific (LKO) *Sec16b* knockout mice exhibit a substantial reduction in serum TG, total cholesterol, and free cholesterol levels due to impaired ApoB lipidation that is partially distinct from MTP-mediated initial lipidation and COPII-mediated VLDL intracellular trafficking. Surprisingly, despite higher hepatic lipid

content, LKO mice show smaller LDs in hepatocytes. Mechanistically, SEC16B localizes to ER-LD contact sites, facilitating the targeting of LD-associated proteins that promote LD expansion. More importantly, loss of *Sec16b* ameliorates hyperlipidemia and reduces lesion areas in *Ldlr* null mice without causing apparent liver damage. These findings reveal a mechanism connecting VLDL and LD metabolism and demonstrate SEC16B as a potential therapeutic target for atherosclerosis.

## Results

### SNP in *SEC16B* is associated with plasma cholesterol levels in humans

GWAS has identified that one of the SNPs (rs6682862, chr1:177969302, Alleles: G>A) located in the promoter region of *SEC16B* is significantly associated with plasma cholesterol levels (Figure 1A) (20, 21). An analysis of expression quantitative trait loci (cis-eQTLs) revealed that the minor allele of rs6682862-A is correlated with increased expression of *SEC16B* in the liver (Figure 1B). To directly test whether different alleles affect *SEC16B* expression, we cloned the promoter region of human *SEC16B* genes (both G allele and A allele) to the upstream of a firefly luciferase reporter gene. Luciferase assay demonstrated that A allele increased luciferase activity by ~4-fold compared to the G allele (Figure 1C), which is consistent with eQTL data. Notably, DNase-Seq and ATAC-Seq analyses showed that rs6682862 resides within the open chromatin promoter region of the *SEC16B* gene on chromosome 1 (Figure 1E), further suggesting its regulatory role in *SEC16B* expression.

### Hepatic *SEC16B* expression is regulated by HNF4A and feeding conditions

Using enrichment analysis in ChIP-Atlas (22), we identified HNF4A as a potential transcription factor that binds to the promoter region of *SEC16B* (Figure 1D). An analysis of ChIP sequencing dataset for HNF4A in the liver revealed two binding peaks in the promoter region of *SEC16B*

gene (Figure 1E). It is noteworthy that HNF4A also binds to the promoter of mouse *Sec16b* gene (Figure 1E). Examination of a published microarray dataset from *Hnf4a* knockout fetal livers showed a substantial reduction in *Sec16b* expression in the absence of HNF4A (Figure 1F) (23). In line with this, *Sec16b* expression was also downregulated by AAV-TBG-CRE-mediated *Hnf4a* acute knockout in the livers of *Hnf4a* floxed mice fed a high fat/cholesterol/fructose (HFCF) diet containing 40% fat/0.2% cholesterol and 4.2% fructose (Figure 1G). Conversely, AAV-mediated overexpression of *HNF4A* markedly increased *Sec16b* expression in the livers of mice on the HFCF diet (Figure 1H). Furthermore, *HNF4A* overexpression markedly enhanced luciferase activity in both A- and G-allele constructs (Figure 1I). These findings demonstrate that HNF4A regulates *SEC16B* expression *in vitro* and *in vivo*.

Previous studies have shown that HNF4A plays a critical role in maintaining lipid homeostasis in the liver (24, 25). Given the strong association between *SEC16B* polymorphism and plasma cholesterol levels, *SEC16B* may function as a downstream target of HNF4A that mediates its effects on lipid metabolism. Gene expression profiling revealed that *SEC16B* is highly expressed in the livers of both humans and mice (Supplemental Figure 1, A and B), the central organ for lipid homeostasis. Furthermore, we found that hepatic *Sec16b* expression was upregulated by fasting and high-fat diet (HFD) feeding (Figure 1, J and K), conditions known to promote lipid accumulation in the liver. Consistently, hepatocytes from obese individuals, who are susceptible to steatosis, expressed higher levels of *SEC16B* (Figure 1L) (26). Similarly, *SEC16B* expression was also elevated in the livers of patients with metabolic-dysfunction associated steatotic liver disease (MASLD) (Figure 1M). Moreover, fatty acid treatment markedly increased *SEC16B* expression in both mouse hepatocytes and Huh7 cells (Figure 1, N and O). Collectively, these

data indicate that SEC16B is responsive to lipid accumulation and likely plays a key role in hepatic lipid metabolism.

***Sec16b* deficiency decreases serum lipids in mice**

To investigate the function of SEC16B *in vivo*, we generated *Sec16b* whole-body knockout (*Sec16b*-/-) mice by crossing heterozygous *Sec16b* $^{tm1a(KOMP)Wtsi}$ (*Sec16b*+/-) mice. Real-time RT-PCR analysis confirmed a more than 95% reduction in *Sec16b* mRNA level in the livers, small intestines, subcutaneous white adipose tissues (sWAT), and muscles of *Sec16b*-/- mice (Supplemental Figure 1C). *Sec16b*-/- mice were viable, fertile, and normal in appearance. Lipid measurement revealed a significant ~25%-50% reduction in serum TG, cholesterol and free cholesterol levels in both male and female *Sec16b*-/- mice compared to controls after 6 hours fasting (Figure 2, A-D), while serum non-esterified fatty acid (NEFA) levels were comparable between groups. Although there was no difference in liver to body weight ratio (Figure 2F), gross appearance, histological analysis and Oil Red O staining indicated increased lipid accumulation in *Sec16b*-/- mice (Figure 2E). This was supported by ~40%-120% increase in hepatic TG, NEFA, and free cholesterol levels (Figure 2, G-H and J), likely due to reduced serum lipid levels.

Given that *Sec16b* is highly expressed in the mouse and human livers (Supplemental Figure 1, A and B), we crossed *Sec16b* floxed (F/F) mice with *Albumin*-Cre mice to generate liver specific knockout (*Sec16b*$^{F/F}$. *Albumin*-Cre, LKO) mice. *Sec16b* mRNA was almost completely depleted in the livers of LKO mice, while the expression of its homolog *Sec16a* remained unaffected (Supplemental Figure 1D). Similar to whole-body knockout mice, both male and female LKO mice exhibited much lower serum TG, total and free cholesterol levels (~30%-55%), but not NEFA levels, compared to control F/F mice after overnight fasting (Figure 2, K-N). Fast protein

liquid chromatography (FPLC) analysis of pooled serum from control and LKO mice showed that hepatic *Sec16b* deletion markedly reduced TG level in VLDL fraction and cholesterol level in HDL fraction (Figure 2, O and P). The gross examination revealed changes consistent with lipid accumulation, including pale livers and a higher liver-to-body weight ratio in LKO mice (Figure 2, Q and S). Lipid accumulation was further confirmed by Oil Red O staining and direct quantification of hepatic lipid content (~45%-100%) (Figure 2R and Figure 2, T-W). Additionally, lipidomics analysis of livers from overnight fasted control and LKO mice corroborated the increases in TG and diacylglycerol (DG) levels but not phospholipids and ceramide (Supplemental Figure 2, A-L). Similar phenotypes were also observed in LKO mice fasted for 6 hours (Supplemental Figure 1, E-H).

**SEC16B modulates VLDL lipidation and secretion**

The marked reduction in serum lipid levels and hepatic lipid accumulation in LKO mice led us to hypothesize that loss of *Sec16b* may hinder VLDL secretion from the liver. To directly assess VLDL secretion, we retro-orbitally injected control and LKO mice with Tyloxapol, which blocks VLDL clearance by inhibiting lipoprotein lipase activity and TG hydrolysis. Remarkably, LKO mice showed a ~60% reduction in TG secretion (Figure 3A). This decrease in TG output can result from compromised ApoB lipidation and/or impaired VLDL secretion. Electron microscopy of negatively stained VLDL fractions revealed much smaller VLDL particles in LKO mice (Figure 3, B and C), indicating impaired ApoB lipidation. Western blot analysis revealed a reduction in serum ApoB levels in both Tyloxapol injected and 16 h fasted LKO mice compared to controls (Figure 3, D and F). To directly quantify ApoB secretion rates, we performed $^{35}S$ labeling assay *in vivo*, which demonstrated that loss of *Sec16b* reduced ApoB secretion by ~25% relative to controls (Figure 3E). Together, these data indicate that hepatic ApoB secretion is

impaired in the absence of SEC16B. In contrast, serum albumin levels were comparable between control and LKO (Figure 3F). Moreover, Coomassie blue and silver staining of serum proteins revealed that most proteins were comparable between the two groups (Supplemental Figure 3A), indicating that SEC16B is unlikely to play a major role in overall protein secretion. Interestingly, despite the reduced secretion of ApoB into serum, ApoB protein and mRNA levels remained unchanged in LKO livers (Figure 3F and Supplemental Figure 3, B and C).

To assess the relevance to humans, we knocked down *SEC16B* in Huh7 human liver cells using shRNA. Consistent with our mouse data, *SEC16B* knockdown reduced ApoB secretion into the medium by ~60% (Supplemental Figure 4A), concomitant with ApoB accumulation in cell lysate, suggesting that SEC16B also regulates ApoB secretion in humans.

ApoB undergoes two stages of lipidation: an initial lipidation facilitated by MTP and a poorly understood bulk lipidation (9). We next investigated whether *Sec16b* deficiency affects the abundance and function of MTP. Western blot and real-time RT-PCR analysis showed no difference in MTP protein and mRNA levels in control and LKO livers (**F**igure 3E and Supplemental Figure 3, B and C). Direct measurement of neutral lipid transfer activity from microsomes isolated from mouse livers and Huh7 cells revealed no significant differences between groups (Supplemental Figure 4, B-D). Additionally, *SEC16B* knockdown reduced ApoB secretion to a similar extent in both DMSO and MTP inhibitor Lomitapide treated Huh7 cells (Supplemental Figure 4A). Interestingly, ApoB accumulated in DMSO treated but not Lomitapide treated cells (Supplemental Figure 4A), likely because ApoB and MTP expression was decreased in Lomitapide-treated *SEC16B* knockdown cells (Supplemental Figure 4, E and F). To further determine whether MTP mediates the ApoB secretion defect caused by *SEC16B* deficiency, we overexpressed MTP in control and *SEC16B* knockdown cells and assessed ApoB

secretion. MTP overexpression enhanced ApoB secretion to a comparable level in both control and knockdown cells (Supplemental Figure 4G). Together, these findings suggest that SEC16B likely regulates ApoB secretion at least partially distinct from MTP-mediated initial lipidation. To gain further insight into the mechanism underlying defective VLDL secretion in *Sec16b* LKO mice, we conducted electron microscopy analysis on control and LKO liver samples. In control hepatocytes, lipoprotein particles (red arrow heads) were easily visualized in the secretory vesicles and Golgi (Figure 3F). In contrast, lipoprotein particles were much smaller and less stained in the secretory vesicles of LKO hepatocytes, further corroborating poor ApoB lipidation in the absence of SEC16B. Notably, we did not detect prominent lipoprotein particles in the Golgi of LKO hepatocytes. Instead, an increase in ER luminal LDs (yellow arrows) was observed in LKO hepatocytes (Figure 3F). To further investigate if SEC16B regulates the intracellular trafficking of VLDL particles, we isolated ER and Golgi fractions from control and LKO livers and analyzed ApoB and TG levels in these fractions. Interestingly, we found increased levels of ApoB-100 in the ER fractions of LKO livers (Figure 3G), suggesting that loss of *Sec16b* likely blocks the trafficking of ApoB from ER to Golgi. Meanwhile, we observed a trend toward a modest increase in TG content in the ER fractions of LKO livers (Figure 3H). These data demonstrate that SEC16B likely regulates VLDL production by facilitating both ApoB lipidation and trafficking to the Golgi in hepatocytes.

**Knockdown of *SEC16B* impairs the interaction between SEC13 and SEC31A, thereby disrupting COPII assembly and ApoB secretion**

VLDL intracellular trafficking is mediated by specialized COPII-coated vesicles that are assembled at designated ER exit sites (ERES) (27). To investigate the molecular mechanisms by which SEC16B regulates VLDL secretion, we measured the protein levels of COPII components

in LKO livers and *SEC16B* knockdown Huh7 cells. Notably, most of these proteins were upregulated in LKO livers and *SEC16B* knockdown Huh7 cells (Supplemental Figure 5, A-C). Consistent with its localization to the ERES (28), SEC16B showed almost complete colocalization with COPII components, including SEC31A, SEC23A and SEC24B, in Huh7 cells (Supplemental Figure 5, D-F). Interestingly, SEC13 only partially colocalized with SEC16B or other COPII components (Supplemental Figure 5, D-F), likely because SEC13 is also a component of the nuclear pore complex and the GATOR complex (29-31).

COPII complex assembly is initiated by the activation of SAR1, which transitions from GDP-bound to GTP-bound state (32, 33). Immunofluorescence analysis using an antibody specific for the GTP-bound SAR1 revealed significantly elevated SAR1-GTP levels in *SEC16B* knockdown Huh7 cells and LKO hepatocytes (Figure 4, A and B), indicating enhanced initiation of COPII vesicle assembly. To further investigate the involvement of SEC16B in SAR1 and COPII-mediated VLDL secretion, we attempted to overexpress SAR1 in Huh7 cells. Of the two SAR1 paralogs, SAR1B is well-established as a key mediator of lipoprotein secretion (34), whereas SAR1A shares partially overlapping functions in COPII-mediated lipoprotein secretion (34, 35). Interestingly, only SAR1A, but not SAR1B, could be robustly overexpressed in Huh7 cells (data not shown). Nevertheless, SAR1A overexpression significantly increased ApoB production and secretion in control Huh7 cells (Figure 4C). In contrast, *SEC16B* knockdown completely abolished the SAR1A-induced increase in ApoB secretion (Figure 4C), indicating that SEC16B is essential for COPII-mediated VLDL trafficking.

Upon activation, SAR1 recruits SEC23 and SEC24 to form the inner layer of the COPII coat, followed by the assembly of the outer layer composed of SEC13 and SEC31 (33). *SEC16B* knockdown did not affect the association between SEC24B and SEC23A, nor the colocalization

between the inner and outer coat components, including SEC31A with SEC24B, and SEC31A with SEC23A (Figure 4, D-H). In contrast, *SEC16B* knockdown impaired the association and interaction between the outer coat components SEC13 and SEC31A (Figure 4, I-L). In yeast, SEC16 interacts with SEC13 through its central conserved domain (CCD) (36, 37). Given that SEC16B shares a similar CCD with yeast SEC16 (28), we hypothesized that SEC16B may interact with SEC13 in mammals. Indeed, co-immunoprecipitation analysis revealed an interaction between SEC16B and SEC13, but not with SAR1A or SEC23A (Figure 4M and Supplemental Figure 5, G and H). These data suggest that SEC16B selectively modulates the assembly of the COPII outer coat complex, likely by interacting with SEC13.

Once the inner and outer COPII coats are fully assembled, SAR1-GTP is hydrolyzed by SEC23, a process accelerated by the outer layer complex (38). This GTP hydrolysis is a crucial step for COPII vesicle scission and release. Our observations of impaired outer coat assembly and elevated SAR1-GTP levels in *SEC16B* knockdown cells suggest that COPII vesicle release may be compromised in the absence of SEC16B. Consistent with this, the association between SEC31A and SAR1A was markedly increased in *SEC16B* knockdown Huh7 cells (Figure 4N), indicating defective vesicle release. To directly visualize COPII dynamics, we performed time lapse microscopy to track the movement of GFP-SEC13-labeled puncta in control and *SEC16B* knockdown cells (Supplemental Video 1-6). Quantitative analysis of the puncta trajectories revealed significant reduction in mean and maximal speed and displacement, as well as a trend toward decreased total travel distances in *SEC16B* knockdown cells (Supplemental Figure 6, A-D). Furthermore, the proportion of moving puncta was also significantly reduced in knockdown cells (Supplemental Figure 6, E-F). Taken together, these findings suggest that SEC16B

promotes VLDL secretion by modulating COPII assembly and its intracellular trafficking, potentially through mediating the interaction between SEC31A and SEC13.

**SEC16B controls hepatic LD expansion**

Impaired VLDL secretion typically leads to LD formation and steatosis in hepatocytes. Histological analysis revealed characteristics of microvesicular steatosis in the livers of both male and female LKO mice after overnight fasting, as manifested by distended hepatocytes with central nuclei and white, foamy-appearing cytoplasm (Figure 5A). Microvesicular steatosis tends to have small LDs, leading us to consider whether *Sec16b* deletion affects LD size. Electron microscopy analysis and quantification of LD size revealed that LKO hepatocytes indeed contained a greater number of smaller LDs than controls (Figure 5, B-E).

Next, we challenged the mice with different diets known to promote lipid accumulation in the liver, including high carbohydrate diet (HCD), HFD, and Western diet (WD). Interestingly, chronic dietary challenges had minimal impacts on serum or hepatic TG or NEFA levels (Supplemental Figure 7, A-C), likely due to their dynamic regulation by different organs, such as liver, intestine and adipose tissues. In contrast, serum cholesterol levels remained significantly reduced in LKO mice fed these diets (Supplemental Figure 7, A-C). Histological analysis showed that LKO livers exhibited prominent microvesicular steatosis without noticeable LDs (Figure 5F). Electron microscopy analysis of WD-fed mouse livers revealed much smaller LDs in LKO mice compared to control mice (Figure 5, G-I). Conversely, overexpression of *Sec16b* in mouse primary hepatocytes increased LD size (Figure 5J-L). To further investigate whether SEC16B regulates LD size in humans, we knocked down *SEC16B* expression in Huh7 cells and observed significantly smaller LDs upon oleic acid treatment (Figure 5, M-O). These data indicate that SEC16B is both necessary and sufficient to modulate LD size in the liver.

**SEC16B partially localizes to ER-LD contact sites and controls protein targeting to LDs**

LDs are classified into three types based on their subcellular localization: cytoplasmic, nuclear and ER luminal LDs (13). To examine if SEC16B affects a specific subset of LDs, we stained for PLIN2, a marker of cytoplasmic LDs, in *SEC16B* knockdown Huh7 cells and LKO hepatocytes. The results showed that most LDs were PLIN2 positive in both control and knockdown or LKO cells, suggesting that the majority of LDs are cytoplasmic and that *Sec16b* deficiency does not alter PLIN2 localization (Supplemental Figure 8, A and B).

The size of cytoplasmic LDs can be regulated by various processes, including lipid biosynthesis/uptake, TG/VLDL secretion, LD catabolism and growth (13, 39). Considering that *Sec16b* deficiency impairs VLDL secretion, which would theoretically lead to increased lipid accumulation and larger LD formation, the presence of smaller LDs in LKO hepatocytes is unlikely caused by impaired VLDL secretion. Gene expression analysis showed no significant differences in the expression of the sterol regulatory element-binding protein 1c (SREBP-1c) and its downstream lipogenic genes or lipid hydrolysis genes after overnight fasting (Supplemental Figure 3, B-D), suggesting that these pathways are unlikely to account for the smaller LDs in the absence of SEC16B. Similarly, the expression of most known genes involved in LD expansion, such as cell death inducing DFFA like effector (*Cide*) family members, diacylglycerol O-acyltransferase 2 (*Dgat2*), glycerol 3-phosphate acyltransferase 4 (*Gpat4*) and acyl-CoA synthetase long chain family member 3 (*Acsl3*) was not significantly altered between control and LKO livers, except for a modest change in *Cideb* and Calsyntenin 3β (*Clstn3b*) mRNA levels in male LKO mice (Supplemental Figure 3, B and C). Western blot analysis of whole liver lysates showed no change in GPAT4 protein levels and a trend toward slightly decreased DGAT2 and

CIDEB protein levels in LKO livers (Supplemental Figure 8D). These data suggest that the effect of *Sec16b* deficiency on LD expansion is unlikely to be driven by altered gene expression.

To further elucidate the mechanism by which SEC16B controls LD size, we first examined the subcellular localization of SEC16B. Immunofluorescence staining revealed that SEC16B was partially localized to the surface of LDs in Huh7 cells (Figure 6, A and B). Notably, co-staining with the ER marker KDEL and LDs showed that some SEC16B signals were localized to the contact sites between the ER and LDs (Figure 6C). Additionally, SEC16B partially overlapped with PLIN2 surrounding LDs (Supplemental Figure 8C). To validate this observation, we fractionated liver samples from Flag-tagged *Sec16b* transgenic mice. Western blot analysis demonstrated the enrichment of SEC16B in both LD and total membrane fractions with high ER content indicated by ER membrane marker CALNEXIN (Figure 6D). Given that ER-LD contact sites mediate protein and lipid transfer between the organelles (13, 40-42), we hypothesized that SEC16B localizes to ER-LD contact sites and facilitates the translocation of LD-associated proteins to LDs, thereby modulating LD expansion. Indeed, silver staining revealed that protein levels normalized to TG content were reduced in LDs purified from LKO livers compared to controls (Supplemental Figure 8E). Interestingly, western blot analysis showed that CIDEB, but not PLIN2 or CALNEXIN, was reduced in LDs from LKO livers normalized to either TG content or total proteins (Supplemental Figure 8, F and G), suggesting that SEC16B may facilitate the translocation of selected proteins to LDs.

Next, we performed proteomics on LDs isolated from control and LKO mouse livers. As expected, the majority of significantly downregulated proteins were associated with LDs and/or ER (Figure 6E and supplemental table 1). Remarkably, proteins such as ACSL3, GPAT4, DGAT2, and CIDEB have been previously reported to translocate to LDs and promote their

expansion (15, 43, 44). To visualize if SEC16B regulates their translocation, we overexpressed these proteins tagged with HA in control and *SEC16B* knockdown Huh7 cells and performed immunofluorescence analysis upon oleic acid treatment. Knockdown of *SEC16B* dramatically reduced the colocalization of these proteins with LDs (Figure 6F). Taken together, these findings demonstrated that SEC16B is a regulator of LD expansion through selectively modulating the translocation of LD-associated proteins.

**Constitutive *Sec16b* knockout ameliorates atherosclerosis**

Genetic, epidemiologic, and clinical studies have established that hyperlipidemia, particularly elevated LDL-C, is a key risk factor for atherosclerosis (6, 45, 46). Given that *Sec16b* deficiency markedly reduces serum lipid levels, we investigated whether loss of *Sec16b* affects atherogenesis. To induce atherosclerosis in mice, we crossed *Sec16b*-/- mice with *Ldlr*-/- mice to generate *Sec16b*+/+ *Ldlr*-/- (control) and *Sec16b*-/- *Ldlr*-/- (DKO) mice, and fed them a WD for 12 weeks. Both male and female mice in the control and DKO groups exhibited similar blood glucose levels and liver-to-body weight ratios (Supplemental Figure 9, B and C). Body weight was comparable in male mice, whereas female DKO mice showed a trend toward increased body weight (P = 0.053) (Supplemental Figure 9A). As expected, deletion of *Ldlr* combined with WD feeding led to a ~10-fold increase in serum TG, cholesterol, and free cholesterol levels. Notably, serum TG, total and free cholesterol levels were significantly reduced by ~30-50% in both male and female DKO mice compared to control mice, while NEFA levels remained comparable between the groups (Figure 7, A-D). FPLC analysis revealed a dramatic reduction in VLDL-TG, as well as VLDL- and LDL-cholesterol in DKO serum compared to controls (Figure 7, E and F). These data also suggest that *Sec16b* deficiency induced serum lipids reduction is independent of LDLR-mediated lipid uptake.

The evaluation of atherosclerotic plaques revealed much smaller aortic lesion area in both male and female DKO mice than controls (Figure 7, G and J). The reduction in plaque area was further confirmed by Oil red O staining of the *en face* aortic arch (Figure 7, H and K) and aortic root sections (Figure 7, I and L). A potential concern with reducing hyperlipidemia by blocking VLDL secretion is the risk of lipid accumulation in the liver, which could lead to MASLD. Indeed, DKO mice exhibited approximately a 60% increase in hepatic TG compared to control mice, while other lipid levels were not altered (Supplemental Figure 9, F-I). Despite more microvesicular steatosis in DKO livers from histological analysis (Supplemental Figure 9D), similar levels of inflammation and fibrosis were observed when compared to control mice (Supplemental Figure 9, D and E). Consistently, the mRNA levels of inflammatory genes (*Tnfa*, *F4/80*, and *Il1b*) and fibrogenic genes (*Col1a1*, *Col3a1* and *Tgfb*) were not altered in DKO mice (Supplemental Figure 9J). Furthermore, no increases in alanine transaminase (ALT) and aspartate transaminase (AST) levels were detected in DKO mice compared to controls (Supplemental Figure 9, K and L). Thus, *Sec16b* deficiency ameliorates atherosclerosis progression without causing noticeable lipotoxicity in the liver.

**Acute deletion of hepatic *Sec16b* delays atherosclerosis progression**

To investigate whether acute deletion of *Sec16b* can mitigate atherosclerosis development and serve as a therapeutic strategy, we crossed *Sec16b* floxed (*Sec16b*$^{F/F}$) mice with *Ldlr*-/- mice to generate *Sec16b*$^{F/F}$ *Ldlr*-/- mice. These mice were fed a WD for 6 weeks to initiate atherosclerosis development, followed by retro-orbital injection with either eGFP or CRE AAV driven by a liver specific TBG promoter, and then continued on the WD for an additional 6 weeks (Supplemental Figure 10A). No significant differences in body weight or blood glucose levels were observed between eGFP AAV- and CRE AAV-injected mice, regardless of sex

(Supplemental Figure 10, B and C). Both male and female mice receiving CRE AAV exhibited ~20-60% reductions in serum TG, total and free cholesterol levels compared to those injected with eGFP (Figure 8, A-C). In contrast, NEFA levels were only reduced in male mice (Figure 8D). Consistently, serum from CRE AAV-injected mice appeared relatively clear compared to the more milky serum of eGFP AAV-injected mice (Figure 8E). FPLC analysis revealed markedly lower TG and cholesterol levels in the VLDL and LDL fractions of CRE AAV-treated mice (Figure 8, F and G).

Aortic lesion areas were dramatically reduced in both male and female mice receiving CRE AAV, as evidenced by direct measurement of plaque area (Figure 8, H and M), Oil Red O staining of the *en face* aortic arch (Figure 8, I and N) and aortic root sections (Figure 8, J and O). Next, we analyzed plaque composition by assessing macrophage and collagen contents. CD68 immunostaining revealed that the percentage of macrophage area relative to the lesion area was comparable between eGFP and CRE AAV injected mice (Figure 8, K and P). Sirius Red staining demonstrated reduced collagen content in the lesions of CRE AAV injected male mice, but not female mice (Figure 8, L and R). Quantification of the necrotic core area, an indicator of plaque stability, showed no difference between eGFP and CRE injected mice, indicating comparable plaque stability between groups (Figure 8Q). Moreover, the necrotic cores comprised a relatively small fraction of the lesion area (~2%), suggesting an early stage of atherosclerosis. These data demonstrated that plaque composition remains largely unchanged between groups, suggesting that hepatic *Sec16b* deficiency reduces plaque burden without modulating the inflammatory status of the atherosclerotic lesion.

Next, we assessed the effect of acute *Sec16b* deletion on the liver. The liver-to-body weight ratio was slightly increased in male CRE AAV-injected mice but not in females (Supplemental Figure

10D). Lipid analysis showed elevated hepatic TG but no changes in other lipids in both male and female CRE AAV-treated mice (Supplemental Figure 10, E-H). H&E staining revealed more microvesicular steatosis in both male and female CRE AAV-injected mice (Supplemental Figure 10K), while eGFP AAV-injected mice exhibited macrovesicular steatosis. Additionally, male mice receiving CRE AAV showed reduced inflammation (Supplemental Figure 10K), which was further supported by decreased mRNA levels of inflammatory genes (*Tnfa* and *Il1b*) (Supplemental Figure 10I). Interestingly, the mRNA levels of fibrogenic genes (*Col1a1* and *Col3a1*) were downregulated in female CRE AAV-injected mice (Supplemental Figure 10J). Moreover, there was no discernible difference in fibrosis between CRE AAV and eGFP AAV-injected mice of either sex, as assessed by Sirius red staining (Supplemental Figure 10L). In agreement with the absence of noticeable liver damage, there was no difference in ALT and AST levels between eGFP AAV and CRE AAV-injected mice (Supplemental Figure 10, M and N). Consistent with the observations in LKO mice, *Sec16b* knockout also reduced LD size in the livers of *Ldlr*$^{-/-}$ mice (Supplemental Figure 10, O and P). These data suggest that SEC16B may represent a potential therapeutic target for hyperlipidemia and atherosclerosis.

**Hepatic *Sec16b* deletion does not affect disease progression in mouse models of metabolic dysfunction-associated steatohepatitis (MASH)**

To further investigate whether *Sec16b* deficiency influences the progression of MASLD or MASH, we fed *Sec16b* LKO mice a MASH-inducing diet that has been shown to closely recapitulate human MASH in mouse livers (47, 48). After 24 weeks of diet feeding, severe steatosis but only mild fibrosis was observed (Supplemental Figure 11, A and B). More pronounced fibrosis was developed in mice subjected to 50 weeks of diet feeding or 24 weeks of MASH diet feeding combined with CCI4 treatment. However, regardless of the feeding regimen

or CCI4 treatment, both control and LKO mice exhibited similar levels of steatosis, fibrosis and inflammation in the liver (Supplemental Figure 11, A and B). Moreover, the mRNA expression of inflammatory genes (*Tnfa*, *F4/80*, and *Il1b*) and fibrogenic genes (*Col1a1*, *Col3a1*, and *Tgfb*) remained unchanged in LKO mice compared to controls (Supplemental Figure 11C). Consistent with other chronic dietary challenges, serum or hepatic TG or NEFA levels were not altered in LKO mice upon MASH diet feeding (Supplemental Figure 11D). Interestingly, serum cholesterol levels were significantly reduced in LKO mice only after 24 weeks of MASH diet feeding (Supplemental Figure 11D), likely due to severe liver injury and impaired hepatic function caused by prolonged MASH diet exposure. Nevertheless, liver enzyme activities (ALT and AST) were found to be comparable between control and LKO mice (Supplemental Figure 11E). These findings demonstrated that SEC16B is unlikely to play a notable role in the development of MASLD and MASH.

**Discussion**

Excess lipids, particularly free fatty acids and cholesterol, are known to cause cellular lipotoxicity. In hepatocytes, free fatty acids and cholesterol can be esterified into TG and cholesterol esters, respectively, which are either stored in LDs or secreted into circulation as VLDL. These tightly regulated processes help prevent hepatic lipid stress and meet the lipid demands of peripheral tissues. However, the mechanism underlying this regulation remains unclear. Through GWAS on human plasma lipids, we identified SEC16B as a vital regulator of both VLDL and LD metabolism. Our data demonstrate that hepatic *Sec16b* deficiency impairs VLDL lipidation and secretion, as well as LD expansion, suggesting that VLDL and LD metabolism may rely on the same machinery in the liver. Notably, hepatic *Sec16b* expression is induced by lipid accumulation in mice subjected to overnight fasting and chronic HFD feeding,

as well as obese and MASLD humans. These findings demonstrate that SEC16B functions as a lipid-responsive regulator in the liver that promotes VLDL secretion and LD expansion, thereby handling lipid flux and maintaining lipid homeostasis. Interestingly, our results indicate that *SEC16B* is a target of HNF4A, one of the most abundant transcription factors and a pivotal regulator of lipid metabolism in the liver (24). This likely accounts for the predominant expression of *Sec16b* in both human and mouse liver and suggests that SEC16B may partially mediate the roles of HNF4A in regulating hepatic lipid metabolism.

VLDL metabolism involves several key steps, including ApoB translation, lipidation, trafficking from the ER to Golgi, and secretion into circulation. MTP plays a crucial role in transferring neutral lipids onto ApoB, forming nascent VLDL particles. Recent studies have identified several factors that modulate MTP activity and thereby influence ApoB lipidation, such as PLA2G12B (49) and PRAP1 (50). It is known that disruption of MTP function reduces ApoB lipidation, leading to its degradation (51, 52). Our *in vivo* analyses in mouse liver, along with *in vitro* experiments in Huh7 cells, suggest that *Sec16b* deficiency does not affect MTP expression or its function. Interestingly, despite the poor lipidation of ApoB in *Sec16b* knockout livers, there is an increased accumulation of ApoB in the ER, which appears to contradict the prevailing notion that unlipidated ApoB is destined for degradation (53, 54). However, this observation aligns with the idea that MTP primarily participates in the initial lipidation of ApoB rather than in the subsequent bulk lipid addition (9, 55, 56). Given the intact MTP activity in the absence of SEC16B, it is possible that partially lipidated ApoB is stabilized in the ER, thereby avoiding degradation. This suggests that SEC16B is primarily involved in the relatively less understood process of bulk lipidation.

SEC16B is the shorter mammalian orthologue of *S. cerevisiae* SEC16, initially recognized as a scaffold protein that organizes ERES through interactions with COPII components (57, 58). In mammalian cells, most research has been focused on SEC16A, the longer orthologue, which is ubiquitously expressed and shares the most similarity with yeast SEC16 (28). Although both SEC16A and SEC16B participate in COPII vesicle assembly and ERES organization, several *in vitro* studies indicate that SEC16B likely has specialized, non-redundant functions (28, 59). While VLDL and protein secretion both depend on COPII vesicles (60), recent studies indicate that VLDL secretion is segregated from general protein secretion upon exiting the ER (61). Indeed, our findings indicate that loss of *Sec16b* in mouse liver does not affect circulating levels of Albumin, the most abundant serum protein secreted by the liver, or the levels of most other serum proteins, indicating that SEC16B is not essential for general protein secretion. Thus, SEC16A may play a more prominent role in COPII-mediated protein secretion in the liver, while SEC16B appears to have a specialized function in regulating lipoprotein secretion.

Mechanistically, we found that SEC16B interacts with SEC13 and facilitates the interaction between SEC31A and SEC13, thereby promoting the assembly of the outer layer of the COPII coat and facilitating VLDL trafficking from the ER to Golgi.

Strikingly, our data demonstrate that SEC16B also regulates LD morphology at ER-LD contact sites, which are believed to facilitate the transfer of proteins and lipids. Since LDs contribute to VLDL lipidation and secretion (9, 18, 19, 39), it is plausible that SEC16B may influence LD-associated VLDL lipidation. SEC16B likely facilitates the localization of proteins, such as ACSL3, GPAT4, DGAT2, and CIDEB, to LDs, thereby mediating the lipid transfer between LDs and VLDL. Notably, deficiency in *Dgat2* or *Cideb* has been shown to reduce serum lipids and impair VLDL secretion (19, 62, 63). Whether the mislocalization of these or other yet

unidentified proteins contributes to the impaired VLDL lipidation in *Sec16b* deficient mice remains to be determined. Nevertheless, further investigation is warranted to elucidate this SEC16B-mediated VLDL bulk lipidation process involving LDs.

The biogenesis and growth of LDs are dynamically regulated in hepatocytes to maintain lipid homeostasis. Our data demonstrate that *Sec16b* deficiency leads to the accumulation of a greater number of smaller LDs, indicating that SEC16B primarily influences LD expansion rather than biogenesis. LD expansion is mediated by LD-associated proteins that either catalyze local TG synthesis or facilitate the fusion of smaller LDs. Specifically, GPAT4 and DGAT2 catalyze TG synthesis on the LD surface, which is considered a crucial step in LD growth (15). Additionally, smaller LDs can fuse to form large LDs through the action of CIDE family proteins (64). These proteins, originally located in the ER, translocate to LDs to mediate expansion. However, the precise mechanism governing their translocation remains elusive. Our studies indicate that SEC16B plays a critical role in regulating their translocation. Notably, a genome-wide screen in *Drosophila* identified components of the ERES, including SEC16-the only homolog of SEC16 in *Drosophila*-as key players in ER-to-LD protein targeting (65). Thus, the role of SEC16 and ERES in LD protein translocation appears to be conserved.

Another important finding of our study is the identification of SEC16B as a potential therapeutic target for atherosclerosis. Recent studies have established VLDL, the precursor lipoprotein of atherogenic TGRL remnants and LDL, as a significant risk factor for atherosclerotic cardiovascular disease (ASCVD) (66, 67). Therefore, targeting VLDL metabolism has emerged as a potential strategy to alleviate hyperlipidemia and reduce ASCVD risk. However, a key limitation of suppressing VLDL secretion is the risk of hepatic lipid accumulation, which could progress to MASLD and MASH. Indeed, Lomitapide and mipomersen, an MTP inhibitor and

ApoB synthesis inhibitor, respectively, have been approved only for patients with homozygous familial hypercholesterolemia due to their adverse effects of hepatic fat accumulation and liver injury (7). In this study, we found that targeting SEC16B may offer a safe strategy to mitigate hyperlipidemia without causing overt adverse effects. Under chronic western, high-fat or high-carbohydrate diet feeding conditions, *Sec16b* LKO mice exhibit no or minimal hepatic lipid accumulation while maintaining significant reduction in serum cholesterol levels. This likely reflects the more complex interplay among different tissues in TG metabolism compared to cholesterol metabolism. Alternatively, *Sec16b* deficient livers may be less efficient in secreting lipids via VLDL in response to acute influx of massive lipids from adipose tissue during fasting, whereas LKO mice may have developed compensatory mechanisms to handle hepatic TG in response to chronic feeding. Notably, *Ldlr*-/- mice lacking *Sec16b* exhibit increased hepatic lipid accumulation. Interestingly, control *Ldlr*-/- mice (*Sec16b*+/+, *Ldlr*-/- mice or AAV-TBG-eGFP injected *Ldlr*-/- mice) show much higher TG levels (~200 mg/g liver weight in Supplemental Figure 9F and 10E) compared to wildtype mice after 12 weeks of western diet feeding (~100 mg/g liver weight in Supplemental Figure 7C), indicating that *Ldlr*-/- itself causes a markedly greater lipid burden on the liver, which is consistent with previous observation (68). It is therefore plausible that compensatory mechanisms in *Sec16b* deficient mice are insufficient to cope with this excessive lipid load in the *Ldlr*-/- background. This may explain why *Sec16b*-/-*Ldlr*-/- or AAV-TBG-CRE injected *Ldlr*-/- mice exhibit higher TG compared with their respective controls. Importantly, despite increased hepatic lipid accumulation in *Ldlr*-/- mice lacking *Sec16b*, we did not observe any apparent liver damage, and the expression of certain inflammatory or fibrogenic genes was even reduced in CRE AAV-injected mice compared to controls. Moreover, loss of *Sec16b* in the liver does not promote MASH progression in mice fed

a MASH-inducing diet. Although the role of hepatic LD expansion in MASH progression remains unclear, one of the most distinctive features of MASLD is the formation of supersized LDs, which can exacerbate disease progression (13). Given that *Sec16b* deficiency impairs LD expansion and leads to microvesicular steatosis, it will be interesting to investigate whether this could contribute to the lack of MASLD progression in LKO mice.

In conclusion, these studies uncover a regulatory mechanism that coordinately controls both VLDL secretion and LD metabolism to maintain lipid homeostasis. Importantly, GWAS suggests an association between *SEC16B* SNPs and plasma cholesterol levels in humans. Our findings provide proof of concept that targeting SEC16B may represent a potentially safe and effective therapeutic strategy for ASCVD, at least in patients without *LDLR* mutation.

## Methods

### Sex as a biological variable

Most experiments were conducted in both male and female mice, and no sex differences were observed. For experiments performed in only one sex, the sex of the animals was specifically indicated in the figure legends.

### Animal studies

*Sec16b*$^{F/F}$(F/F) mice have been described (69). *Sec16b* liver-specific knockout (LKO) mice were generated by crossing *Sec16b*$^{F/F}$(F/F) mice with *Albumin-Cre* transgenic mice from The Jackson Laboratory (003574). *Sec16b*-/- mice and *Sec16b*$^{F/F}$ (F/F) were crossed with *Ldlr*-/- (The Jackson Laboratory, 002207) to produce *Sec16b*-/- *Ldlr*-/- and *Sec16b*$^{F/F}$(F/F) *Ldlr*-/- mice. *Hnf4α* floxed mice were obtained from The Jackson Laboratory (#004665). *HNF4*α overexpression were achieved by intravenous injection of AAV8-ALB-h*HNF4α* as previously described (70).

All mice were housed under pathogen-free conditions in a temperature-controlled room with a 12-hour light/dark cycle and had free access to water and a normal chow diet. In most experiment, both male and female mice (8 to 20 weeks old) were used. Experiments conducted in only one sex were specifically indicated in the figure legends. For studies with special diets, 8-weeks-old mice were placed on HFD (60% calories from fat, Research Diets #D12492), HCD (70% carbohydrate diet, TD.98090), or WD (RD Western Diet, Research Diets #D12079B). For MASH studies, 8-weeks-old control and *Sec16b* LKO mice were placed on MASH diet (21.1% fat, 41% sucrose, and 1.25% cholesterol, Teklad diets, TD. 120528) supplemented with 23.1 g/L d-fructose and 18.9 g/L d-glucose in the drinking water for indicated weeks, or combined with weekly CCI4 IP injection as described previously (48). *Hnf4a* LKO and *HNF4α* overexpression mice were fed a high fat/cholesterol/fructose (HFCF) diet containing 40% fat/0.2% cholesterol (from TestDiet, AIN-76A), and 4.2% fructose (in drinking water) for 20 weeks (70). All mice were fasted for 6 h or overnight prior sacrificing as stated in the figure legends.
Additional details on the methods used in this study can be found in the Supplemental Methods.

**Statistical analysis**

Quantifications of immunoblotting and atherosclerosis lesion area were conducted in ImageJ. No statistical methods were used to predetermine sample size. Values were presented as mean ± SEM, as indicated in the figure legends. Statistical analyses were performed by GraphPad Prism10. Statistical significance was calculated by two-tailed Student's t-test, Mann-Whitney test, one-way ANOVA test with the post-hoc test of Tukey or two-way ANOVA test with Sidak's multiple comparisons test, as indicated in the figure legends. Results are considered significant when $P < 0.05$. Asterisks denote corresponding statistical significance *$P < 0.05$, **$P < 0.01$, ***$P < 0.001$ and ****$P < 0.0001$. For mouse experiments, 'n' corresponds to the number of

mice used. For cell culture experiments, ‘n’ corresponds to the number of independent repeats. For cell culture qPCR and western blotting, each sample within each biological replicate corresponds to one well from a tissue culture plate. For mouse liver western blotting, each band corresponds to the protein extract from one mouse.

**Study approval**

Animal housing and all the experimental procedures were approved by the Institutional Animal Care and Use Committee (IACUC) at the University of Illinois at Urbana–Champaign (UIUC) (Protocol #24157 and 24019).

**Data availability**

All data are available in the main text, supplement, and Supporting Data Values. Proteomics data have been deposited to the ProteomeXchange Consortium via the PRIDE partner repository as PRIDE: PXD056229. This paper uses existing, publicly available data from ChIP-Atlas (SRX2636009, SRX10475653, SRX9853116, SRX4497837, SRX681494 and SRX7860740), ENCODE (ENCFF552YJA and ENCFF798FMB) and GEO (GSE3126). Liver eQTL data are from the GTEx project. The lipidomics data are available from the corresponding author on request.

**Author contributions**

W.L. and Z.Z. designed and performed experiments, analyzed data, and wrote the paper. D.M., H.F. R.S., Y.T., T.Y., X.Z., and R.G. performed experiments and analyzed data. Y.Z. K.Z. and J.A. designed experiments and analyzed data. B.W. conceived the project, designed and performed experiments, analyzed data, supervised the project, and wrote the paper.

**Funding support**

This work is the result of NIH funding, in whole or in part, and is subject to the NIH Public

Access Policy. Through acceptance of this federal funding, the NIH has been given a right to make the work publicly available in PubMed Central.

- NIH grants K01DK114373, R01DK128167 and R01HL180740 (to BW).
- NIH grant R01HL147252 (to JA).
- NIH grants R01GM132438 and R01MH124827 (to KZ).
- National Science Foundation (NSF) grant No. 2121003 (to KZ).
- NSF Science and Technology Center for Quantitative Cell Biology grant No. 2243257 (to KZ).
- Start-up funds from University of Illinois Urbana Champaign (to BW).
- Cancer Center at Illinois seed grant (to BW).
- Pfizer Global Medical Grant (70228131) (to BW).
- Burnsides Laboratory Research Fund (to BW).
- USDA grant (W5002) (to JA)

**Acknowledgments**

The authors thank Karen Doty at the Comparative Biosciences Histology Laboratory, and Figen A. Seiler at Electron Microscopy Core of University of Illinois at Chicago for technical support with histology analysis and electron microscopy analysis. We thank Dr. Kalpana Ghoshal (The Ohio State University) for sharing Huh7 cell line. We thank Dr. Benjamin Glick (University of Chicago) for sharing pcDNA-SEC13-GFP plasmid. Lipidomics and proteomics analysis were performed by metabolomics and proteomics core facility of Roy J. Carver Biotechnology Center (CBC) at University of Illinois Urbana Champaign. W.L. was a recipient of a doctoral fellowship from the China Scholarship Council (CSC). Graphic abstract was created with BioRender.

**References**

1. Brunt EM, Wong VW, Nobili V, Day CP, Sookoian S, Maher JJ, et al. Nonalcoholic fatty liver disease. *Nat Rev Dis Primers.* 2015;1:15080.
2. Libby P. Triglycerides on the rise: should we swap seats on the seesaw? *Eur Heart J.* 2015;36(13):774-6.
3. Libby P. The changing landscape of atherosclerosis. *Nature.* 2021;592(7855):524-33.
4. Ference BA, Ginsberg HN, Graham I, Ray KK, Packard CJ, Bruckert E, et al. Low-density lipoproteins cause atherosclerotic cardiovascular disease. 1. Evidence from genetic, epidemiologic, and clinical studies. A consensus statement from the European Atherosclerosis Society Consensus Panel. *Eur Heart J.* 2017;38(32):2459-72.
5. Goldstein JL, and Brown MS. A century of cholesterol and coronaries: from plaques to genes to statins. *Cell.* 2015;161(1):161-72.
6. Musunuru K, and Kathiresan S. Surprises From Genetic Analyses of Lipid Risk Factors for Atherosclerosis. *Circ Res.* 2016;118(4):579-85.
7. Rader DJ, and Kastelein JJ. Lomitapide and mipomersen: two first-in-class drugs for reducing low-density lipoprotein cholesterol in patients with homozygous familial hypercholesterolemia. *Circulation.* 2014;129(9):1022-32.
8. Alves-Bezerra M, and Cohen DE. Triglyceride Metabolism in the Liver. *Compr Physiol.* 2017;8(1):1-8.
9. van Zwol W, van de Sluis B, Ginsberg HN, and Kuivenhoven JA. VLDL Biogenesis and Secretion: It Takes a Village. *Circ Res.* 2024;134(2):226-44.
10. Gordon DA, Wetterau JR, and Gregg RE. Microsomal triglyceride transfer protein: a protein complex required for the assembly of lipoprotein particles. *Trends Cell Biol.* 1995;5(8):317-21.

11. Mansbach CM, and Dowell R. Effect of increasing lipid loads on the ability of the endoplasmic reticulum to transport lipid to the Golgi. *J Lipid Res.* 2000;41(4):605-12.

12. Siddiqi S, Saleem U, Abumrad NA, Davidson NO, Storch J, Siddiqi SA, et al. A novel multiprotein complex is required to generate the prechylomicron transport vesicle from intestinal ER. *J Lipid Res.* 2010;51(7):1918-28.

13. Zadoorian A, Du X, and Yang H. Lipid droplet biogenesis and functions in health and disease. *Nat Rev Endocrinol.* 2023;19(8):443-59.

14. Walther TC, Chung J, and Farese RV, Jr. Lipid Droplet Biogenesis. *Annu Rev Cell Dev Biol.* 2017;33:491-510.

15. Wilfling F, Wang H, Haas JT, Krahmer N, Gould TJ, Uchida A, et al. Triacylglycerol synthesis enzymes mediate lipid droplet growth by relocalizing from the ER to lipid droplets. *Dev Cell.* 2013;24(4):384-99.

16. Gong J, Sun Z, Wu L, Xu W, Schieber N, Xu D, et al. Fsp27 promotes lipid droplet growth by lipid exchange and transfer at lipid droplet contact sites. *J Cell Biol.* 2011;195(6):953-63.

17. Gao M, Huang X, Song BL, and Yang H. The biogenesis of lipid droplets: Lipids take center stage. *Prog Lipid Res.* 2019;75:100989.

18. Yao Z, Zhou H, Figeys D, Wang Y, and Sundaram M. Microsome-associated lumenal lipid droplets in the regulation of lipoprotein secretion. *Curr Opin Lipidol.* 2013;24(2):160-70.

19. Ye J, Li JZ, Liu Y, Li X, Yang T, Ma X, et al. Cideb, an ER- and lipid droplet-associated protein, mediates VLDL lipidation and maturation by interacting with apolipoprotein B. *Cell Metab.* 2009;9(2):177-90.

20. Graham SE, Clarke SL, Wu KH, Kanoni S, Zajac GJM, Ramdas S, et al. The power of genetic diversity in genome-wide association studies of lipids. *Nature.* 2021;600(7890):675-9.

21. Sollis E, Mosaku A, Abid A, Buniello A, Cerezo M, Gil L, et al. The NHGRI-EBI GWAS Catalog: knowledgebase and deposition resource. *Nucleic Acids Res.* 2023;51(D1):D977-D85.

22. Zou Z, Ohta T, and Oki S. ChIP-Atlas 3.0: a data-mining suite to explore chromosome architecture together with large-scale regulome data. *Nucleic Acids Res.* 2024;52(W1):W45-W53.

23. Battle MA, Konopka G, Parviz F, Gaggl AL, Yang C, Sladek FM, et al. Hepatocyte nuclear factor 4alpha orchestrates expression of cell adhesion proteins during the epithelial transformation of the developing liver. *Proc Natl Acad Sci U S A.* 2006;103(22):8419-24.

24. Hayhurst GP, Lee YH, Lambert G, Ward JM, and Gonzalez FJ. Hepatocyte nuclear factor 4alpha (nuclear receptor 2A1) is essential for maintenance of hepatic gene expression and lipid homeostasis. *Mol Cell Biol.* 2001;21(4):1393-403.

25. Thymiakou E, Othman A, Hornemann T, and Kardassis D. Defects in High Density Lipoprotein metabolism and hepatic steatosis in mice with liver-specific ablation of Hepatocyte Nuclear Factor 4A. *Metabolism.* 2020;110:154307.

26. Guilliams M, Bonnardel J, Haest B, Vanderborght B, Wagner C, Remmerie A, et al. Spatial proteogenomics reveals distinct and evolutionarily conserved hepatic macrophage niches. *Cell.* 2022;185(2):379-96 e38.

27. Gillon AD, Latham CF, and Miller EA. Vesicle-mediated ER export of proteins and lipids. *Biochim Biophys Acta.* 2012;1821(8):1040-9.

28. Bhattacharyya D, and Glick BS. Two mammalian Sec16 homologues have nonredundant functions in endoplasmic reticulum (ER) export and transitional ER organization. *Mol Biol Cell.* 2007;18(3):839-49.

29. Valenstein ML, Rogala KB, Lalgudi PV, Brignole EJ, Gu X, Saxton RA, et al. Structure of the nutrient-sensing hub GATOR2. *Nature.* 2022;607(7919):610-6.

30. Enninga J, Levay A, and Fontoura BM. Sec13 shuttles between the nucleus and the cytoplasm and stably interacts with Nup96 at the nuclear pore complex. *Mol Cell Biol.* 2003;23(20):7271-84.

31. Siniossoglou S, Wimmer C, Rieger M, Doye V, Tekotte H, Weise C, et al. A novel complex of nucleoporins, which includes Sec13p and a Sec13p homolog, is essential for normal nuclear pores. *Cell.* 1996;84(2):265-75.

32. Bonifacino JS, and Glick BS. The mechanisms of vesicle budding and fusion. *Cell.* 2004;116(2):153-66.

33. D'Arcangelo JG, Stahmer KR, and Miller EA. Vesicle-mediated export from the ER: COPII coat function and regulation. *Biochim Biophys Acta.* 2013;1833(11):2464-72.

34. Sane AT, Seidman E, Peretti N, Kleme ML, Delvin E, Deslandres C, et al. Understanding Chylomicron Retention Disease Through Sar1b Gtpase Gene Disruption: Insight From Cell Culture. *Arterioscler Thromb Vasc Biol.* 2017;37(12):2243-51.

35. Tang VT, Xiang J, Chen Z, McCormick J, Abbineni PS, Chen XW, et al. Functional overlap between the mammalian Sar1a and Sar1b paralogs in vivo. *Proc Natl Acad Sci U S A.* 2024;121(19):e2322164121.

36. Whittle JR, and Schwartz TU. Structure of the Sec13-Sec16 edge element, a template for assembly of the COPII vesicle coat. *J Cell Biol.* 2010;190(3):347-61.

37. Hughes H, Budnik A, Schmidt K, Palmer KJ, Mantell J, Noakes C, et al. Organisation of human ER-exit sites: requirements for the localisation of Sec16 to transitional ER. *J Cell Sci.* 2009;122(Pt 16):2924-34.

38. Van der Verren SE, and Zanetti G. The small GTPase Sar1, control centre of COPII trafficking. *FEBS Lett.* 2023;597(6):865-82.

39. Mathiowetz AJ, and Olzmann JA. Lipid droplets and cellular lipid flux. *Nat Cell Biol.* 2024;26(3):331-45.

40. Prinz WA, Toulmay A, and Balla T. The functional universe of membrane contact sites. *Nat Rev Mol Cell Biol.* 2020;21(1):7-24.

41. Olzmann JA, and Carvalho P. Dynamics and functions of lipid droplets. *Nat Rev Mol Cell Biol.* 2019;20(3):137-55.

42. Voeltz GK, Sawyer EM, Hajnoczky G, and Prinz WA. Making the connection: How membrane contact sites have changed our view of organelle biology. *Cell.* 2024;187(2):257-70.

43. Xu W, Wu L, Yu M, Chen FJ, Arshad M, Xia X, et al. Differential Roles of Cell Death-inducing DNA Fragmentation Factor-alpha-like Effector (CIDE) Proteins in Promoting Lipid Droplet Fusion and Growth in Subpopulations of Hepatocytes. *J Biol Chem.* 2016;291(9):4282-93.

44. Kassan A, Herms A, Fernandez-Vidal A, Bosch M, Schieber NL, Reddy BJ, et al. Acyl-CoA synthetase 3 promotes lipid droplet biogenesis in ER microdomains. *J Cell Biol.* 2013;203(6):985-1001.

45. Defesche JC, Gidding SS, Harada-Shiba M, Hegele RA, Santos RD, and Wierzbicki AS. Familial hypercholesterolaemia. *Nat Rev Dis Primers.* 2017;3:17093.

46. Do R, Willer CJ, Schmidt EM, Sengupta S, Gao C, Peloso GM, et al. Common variants associated with plasma triglycerides and risk for coronary artery disease. *Nat Genet.* 2013;45(11):1345-52.

47. Tian Y, Jellinek MJ, Mehta K, Seok SM, Kuo SH, Lu W, et al. Membrane phospholipid remodeling modulates nonalcoholic steatohepatitis progression by regulating mitochondrial homeostasis. *Hepatology.* 2024;79(4):882-97.

48. Tsuchida T, Lee YA, Fujiwara N, Ybanez M, Allen B, Martins S, et al. A simple diet- and chemical-induced murine NASH model with rapid progression of steatohepatitis, fibrosis and liver cancer. *J Hepatol.* 2018;69(2):385-95.

49. Thierer JH, Foresti O, Yadav PK, Wilson MH, Moll TOC, Shen MC, et al. Pla2g12b drives expansion of triglyceride-rich lipoproteins. *Nat Commun.* 2024;15(1):2095.

50. Peng H, Chiu TY, Liang YJ, Lee CJ, Liu CS, Suen CS, et al. PRAP1 is a novel lipid-binding protein that promotes lipid absorption by facilitating MTTP-mediated lipid transport. *J Biol Chem.* 2021;296:100052.

51. Liao W, Hui TY, Young SG, and Davis RA. Blocking microsomal triglyceride transfer protein interferes with apoB secretion without causing retention or stress in the ER. *J Lipid Res.* 2003;44(5):978-85.

52. Hussain MM, Shi J, and Dreizen P. Microsomal triglyceride transfer protein and its role in apoB-lipoprotein assembly. *J Lipid Res.* 2003;44(1):22-32.

53. Brodsky JL, and Fisher EA. The many intersecting pathways underlying apolipoprotein B secretion and degradation. *Trends Endocrinol Metab.* 2008;19(7):254-9.

54. Fisher EA, and Ginsberg HN. Complexity in the secretory pathway: the assembly and secretion of apolipoprotein B-containing lipoproteins. *J Biol Chem.* 2002;277(20):17377-80.

55. Gordon DA, Jamil H, Gregg RE, Olofsson SO, and Boren J. Inhibition of the microsomal triglyceride transfer protein blocks the first step of apolipoprotein B lipoprotein assembly but not the addition of bulk core lipids in the second step. *J Biol Chem.* 1996;271(51):33047-53.

56. Rustaeus S, Lindberg K, Stillemark P, Claesson C, Asp L, Larsson T, et al. Assembly of very low density lipoprotein: a two-step process of apolipoprotein B core lipidation. *J Nutr.* 1999;129(2S Suppl):463S-6S.

57. Novick P, Field C, and Schekman R. Identification of 23 complementation groups required for post-translational events in the yeast secretory pathway. *Cell.* 1980;21(1):205-15.

58. Espenshade P, Gimeno RE, Holzmacher E, Teung P, and Kaiser CA. Yeast SEC16 gene encodes a multidomain vesicle coat protein that interacts with Sec23p. *J Cell Biol.* 1995;131(2):311-24.

59. Budnik A, Heesom KJ, and Stephens DJ. Characterization of human Sec16B: indications of specialized, non-redundant functions. *Sci Rep.* 2011;1:77.

60. Tiwari S, and Siddiqi SA. Intracellular trafficking and secretion of VLDL. *Arterioscler Thromb Vasc Biol.* 2012;32(5):1079-86.

61. Wang X, Wang H, Xu B, Huang D, Nie C, Pu L, et al. Receptor-Mediated ER Export of Lipoproteins Controls Lipid Homeostasis in Mice and Humans. *Cell Metab.* 2021;33(2):350-66 e7.

62. Rong S, Xia M, Vale G, Wang S, Kim CW, Li S, et al. DGAT2 inhibition blocks SREBP-1 cleavage and improves hepatic steatosis by increasing phosphatidylethanolamine in the ER. *Cell Metab.* 2024;36(3):617-29 e7.

63. Gluchowski NL, Gabriel KR, Chitraju C, Bronson RT, Mejhert N, Boland S, et al. Hepatocyte Deletion of Triglyceride-Synthesis Enzyme Acyl CoA: Diacylglycerol Acyltransferase 2 Reduces Steatosis Without Increasing Inflammation or Fibrosis in Mice. *Hepatology.* 2019;70(6):1972-85.

64. Gao G, Chen FJ, Zhou L, Su L, Xu D, Xu L, et al. Control of lipid droplet fusion and growth by CIDE family proteins. *Biochim Biophys Acta Mol Cell Biol Lipids.* 2017;1862(10 Pt B):1197-204.

65. Song J, Mizrak A, Lee CW, Cicconet M, Lai ZW, Tang WC, et al. Identification of two pathways mediating protein targeting from ER to lipid droplets. *Nat Cell Biol.* 2022;24(9):1364-77.

66. Seehusen KE, Remaley AT, Sampson M, Meeusen JW, Larson NB, Decker PA, et al. Discordance Between Very Low-Density Lipoprotein Cholesterol and Low-Density Lipoprotein Cholesterol Increases Cardiovascular Disease Risk in a Geographically Defined Cohort. *J Am Heart Assoc.* 2024;13(8):e031878.

67. Zhao F, Qi Y, Liu J, Wang W, Xie W, Sun J, et al. Low Very low-Density Lipoprotein Cholesterol but High Very low-Density Lipoprotein Receptor mRNA Expression in Peripheral White Blood Cells: An Atherogenic Phenotype for Atherosclerosis in a Community-Based Population. *EBioMedicine.* 2017;25:136-42.

68. Bieghs V, Van Gorp PJ, Wouters K, Hendrikx T, Gijbels MJ, van Bilsen M, et al. LDL receptor knock-out mice are a physiological model particularly vulnerable to study the onset of inflammation in non-alcoholic fatty liver disease. *PLoS One.* 2012;7(1):e30668.

69. Shi R, Lu W, Tian Y, and Wang B. Intestinal SEC16B modulates obesity by regulating chylomicron metabolism. *Mol Metab.* 2023;70:101693.

70. Xu Y, Zhu Y, Hu S, Xu Y, Stroup D, Pan X, et al. Hepatocyte Nuclear Factor 4alpha Prevents the Steatosis-to-NASH Progression by Regulating p53 and Bile Acid Signaling (in mice). *Hepatology.* 2021;73(6):2251-65.

## Figures

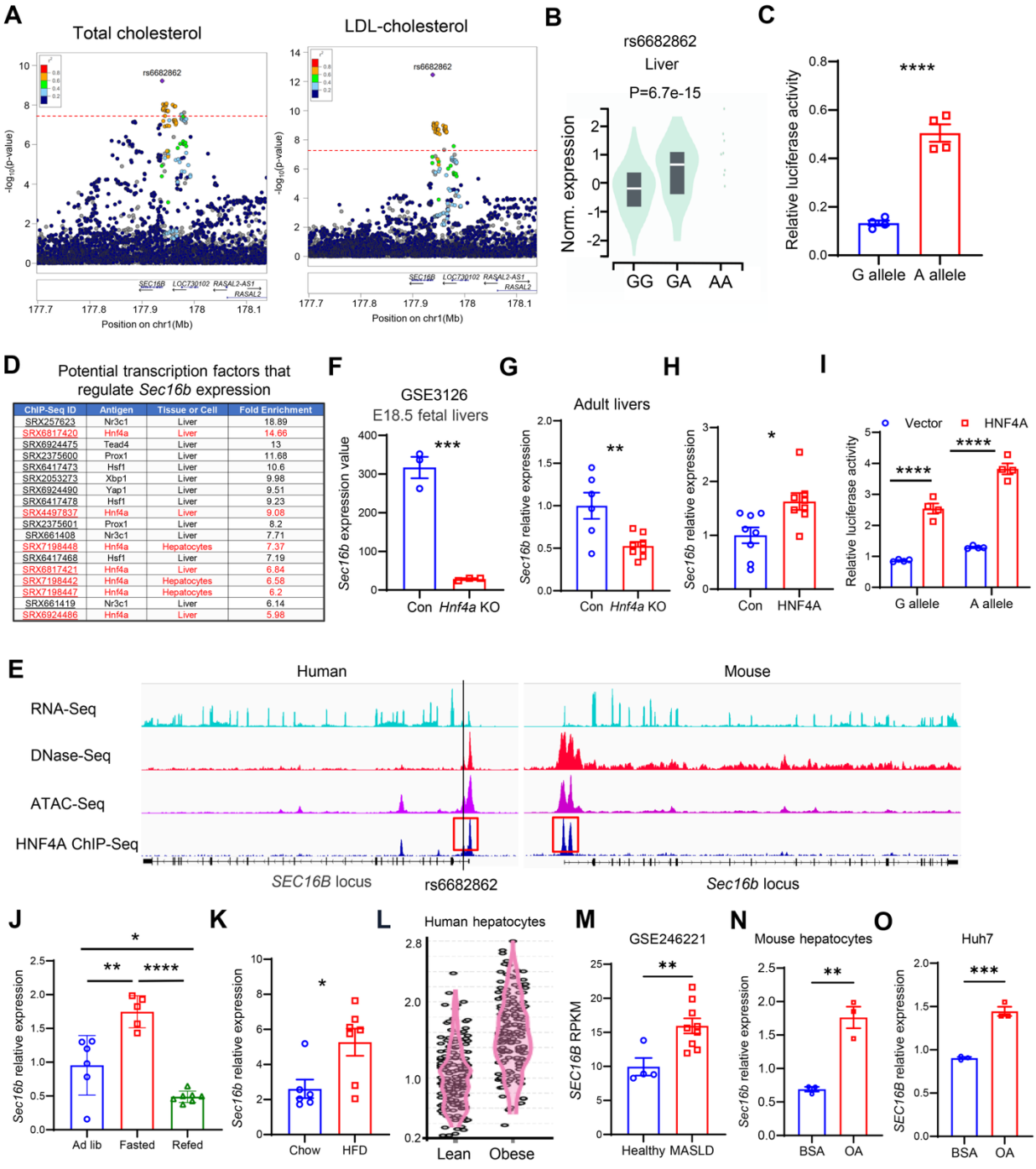


**Figure 1: Association between SNPs in *SEC16B* gene and plasma cholesterol in humans and its expression regulation.**

**(A)** Regional plot of *SEC16B* associated with plasma total cholesterol and LDL-cholesterol levels in humans. Red line indicates the threshold of genome-wide significance ($P = 5x10^{-8}$).

**(B)** eQTL studies showing a highly significant correlation between rs6682862 and *SEC16B* expression in the liver.

**(C)** Luciferase activity of *SEC16B* promoter carrying G and A alleles in HEK-293 cells (n=4).

**(D)** Enrichment analysis showing candidate transcription factors that may bind to 1000 bp up- or downstream of *Sec16b* Transcription Start sites (TSS) in mouse livers. Data are from ChIP atlas.

**(E)** RNA-, DNase-, ATAC- and HNF4A Chip-Seq reads at the *SEC16B* locus of human and mouse liver.

**(F-G)** *Sec16b* mRNA levels in fetal (F) and adult male (G) *Hnf4a* KO mouse livers (f: n=3, g: n=6-8). 8 weeks old mice were fed a HFCF diet for 20 weeks (G).

**(H)** *Sec16b* mRNA levels in male *HNF4A* overexpression mouse livers (n=8). 8 weeks old mice were fed a HFCF diet for 20 weeks.

**(I)** Luciferase activity of *SEC16B* promoter carrying G and A alleles in control and *HNF4A* overexpressing HEK-293 cells (n=4).

**(J)** *Sec16b* mRNA levels in the livers of ad lib fed, fasted, and refed male mice (n=5-7). 8 weeks old mice were fasted for 12 h or fasted for 12 h and refed HCD for 12 h.

**(K)** *Sec16b* mRNA levels in the livers of 8 weeks old male mice fed chow or high-fat diet (HFD) for 12 weeks (n=6-7).

**(L)** *SEC16B* expression in lean and obese hepatocytes. Data are from Liver Cell Atlas.

**(M)** *SEC16B* expression in the livers of healthy donors and MASLD patients.

**(N)** *Sec16b* mRNA levels in mouse primary hepatocytes treated with BSA and 200 μM OA.

**(O)** *SEC16B* mRNA levels in Huh7 cells treated with BSA and 200 μM OA.

Values are means ± SEM or violin plot. Statistical analysis was performed with Student's t test (C, F-H, K and M-O), one-way ANOVA (J) and two-way ANOVA (I). *P < 0.05, **P < 0.01, ***P < 0.001, ****P < 0.0001.

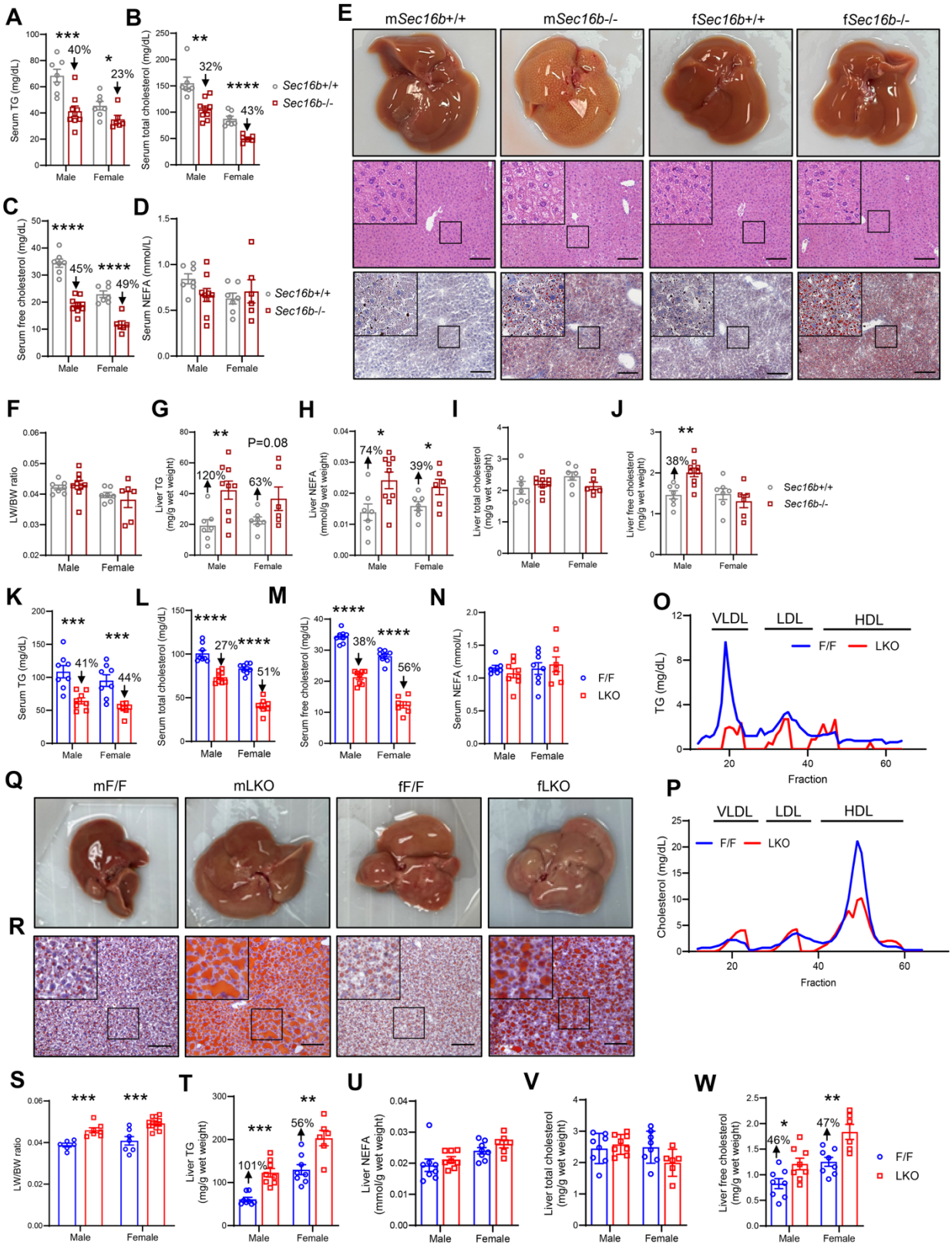


**Figure 2: Loss of *Sec16b* reduces serum lipids and leads to hepatic lipid accumulation.**

**(A-D)** Serum lipid levels in *Sec16b*+/+ and *Sec16b*-/- mice after 6 h fasting (n=6-9).

**(E)** Representative gross images, H&E and Oil Red O staining of livers from *Sec16b*+/+ and *Sec16b-/-* mice fasted for 6 h (n=3). Scale bar = 100 μm.

**(F)** Liver to body weight ratio of *Sec16b*+/+ and *Sec16b-/-* mice fasted for 6 h (n=6-9).

**(G-J)** Hepatic lipid levels of *Sec16b*+/+ and *Sec16b-/-* mice fasted for 6 h (n= 6-9).

**(K-N)** Serum lipid levels in control (*Sec16b*$^{F/F}$, F/F) and LKO (*Sec16b*$^{F/F}$, *Albumin*-Cre) mice after 16 h fasting (n=7-8).

**(O-P)** FPLC analysis of lipoprotein profiles of serum from male control (F/F) and LKO mice fasted for 16 h. Serum from 7 mice/group was pooled.

**(Q-R)** Representative gross images (Q) and Oil-Red-O staining (R) of livers from control (F/F) and LKO mice fasted for 16 h. Scale bar = 100 μm.

**(S-W)** Liver/body weight ratio and hepatic lipid levels of control (F/F) and LKO mice fasted for 16 h (n=6-13).

Values are means ± SEM. Statistical analysis was performed with Student's t test. *P < 0.05, **P < 0.01, ***P < 0.001, ****P < 0.0001.

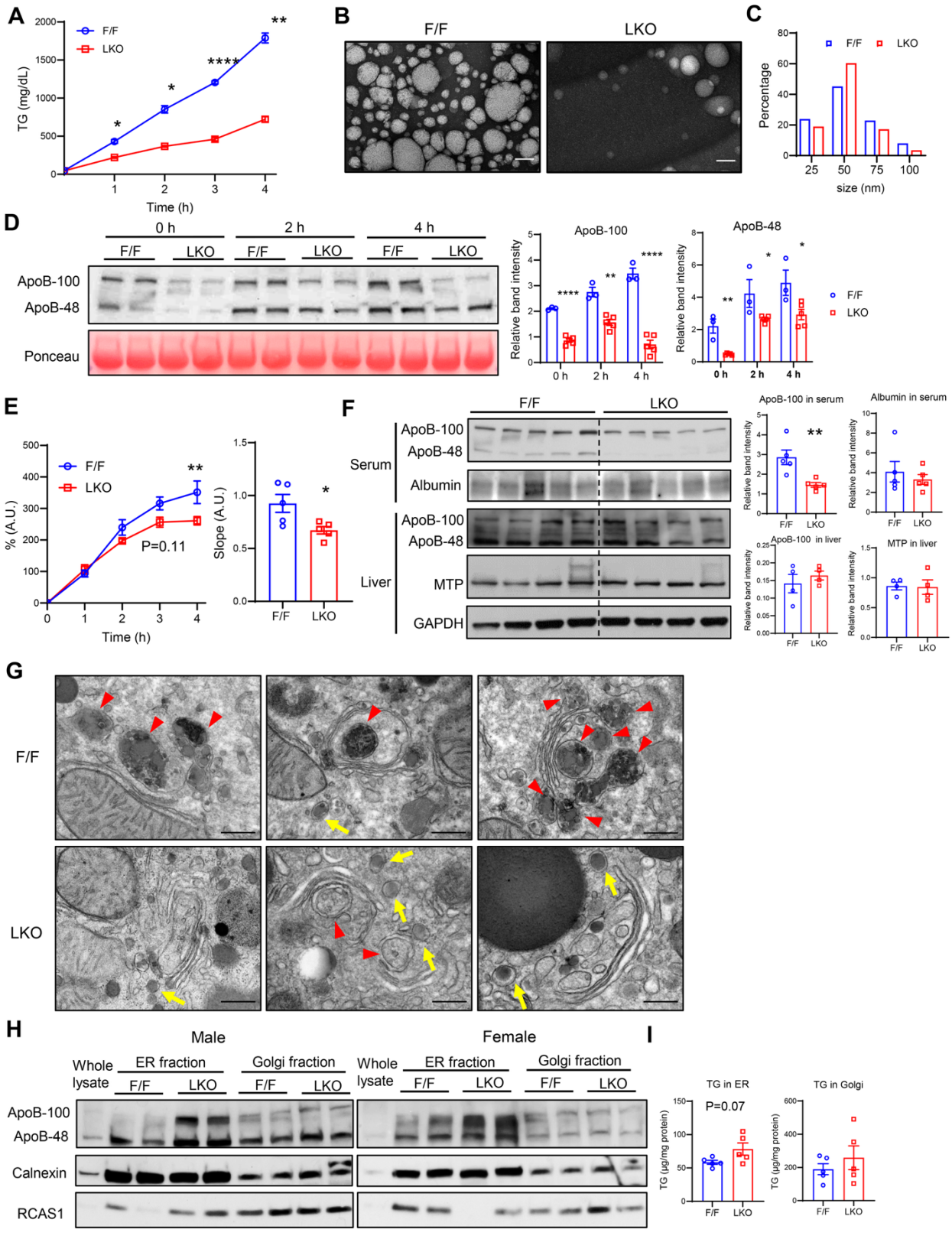


**Figure 3: Hepatic *Sec16b* deficiency impairs ApoB lipidation and VLDL secretion.**

**(A)** VLDL-TG secretion in control (F/F) and LKO female mice. Mice were fasted for 4 h followed by Tyloxapol injection. Serum TG levels were measured at indicated time points (n=3-5).

**(B-C)** Negative staining and quantification of serum VLDL particle size in control (F/F) and LKO mice as in A. Scale bar = 100 nm.

**(D)** Representative western blot image and quantification of serum ApoB levels in control (F/F) and LKO mice as in A.

**(E)** Quantification of $^{35}S$ labeled ApoB-100 secretion rates in Tyloxapol injected male and female control (F/F) and LKO mice (n=5/group).

**(F)** Western blot analysis and quantification of ApoB, Albumin and MTP in the serum and livers of male control (F/F) and LKO mice after 16 h fasting.

**(G)** Electron microscopy analysis of liver sections from male control (F/F) and LKO mice after 16 h fasting (n=3). Red arrow heads indicate VLDL secretory vesicles. Yellow arrows indicate LDs in the ER. Scale bar = 400 nm.

**(H)** Western blot analysis of ApoB in whole lysate, ER and Golgi fractions of livers from control (F/F) and LKO mice after 16 h fasting.

**(I)** Triglyceride levels in the ER and Golgi fractions of livers from male control (F/F) and LKO mice fasted for 16 h (n=5).

Values are means ± SEM. Statistical analysis was performed with Student's t test (D, E (slope), F and I) and two-way ANOVA (A and E). *P < 0.05, **P < 0.01, ****P < 0.0001.

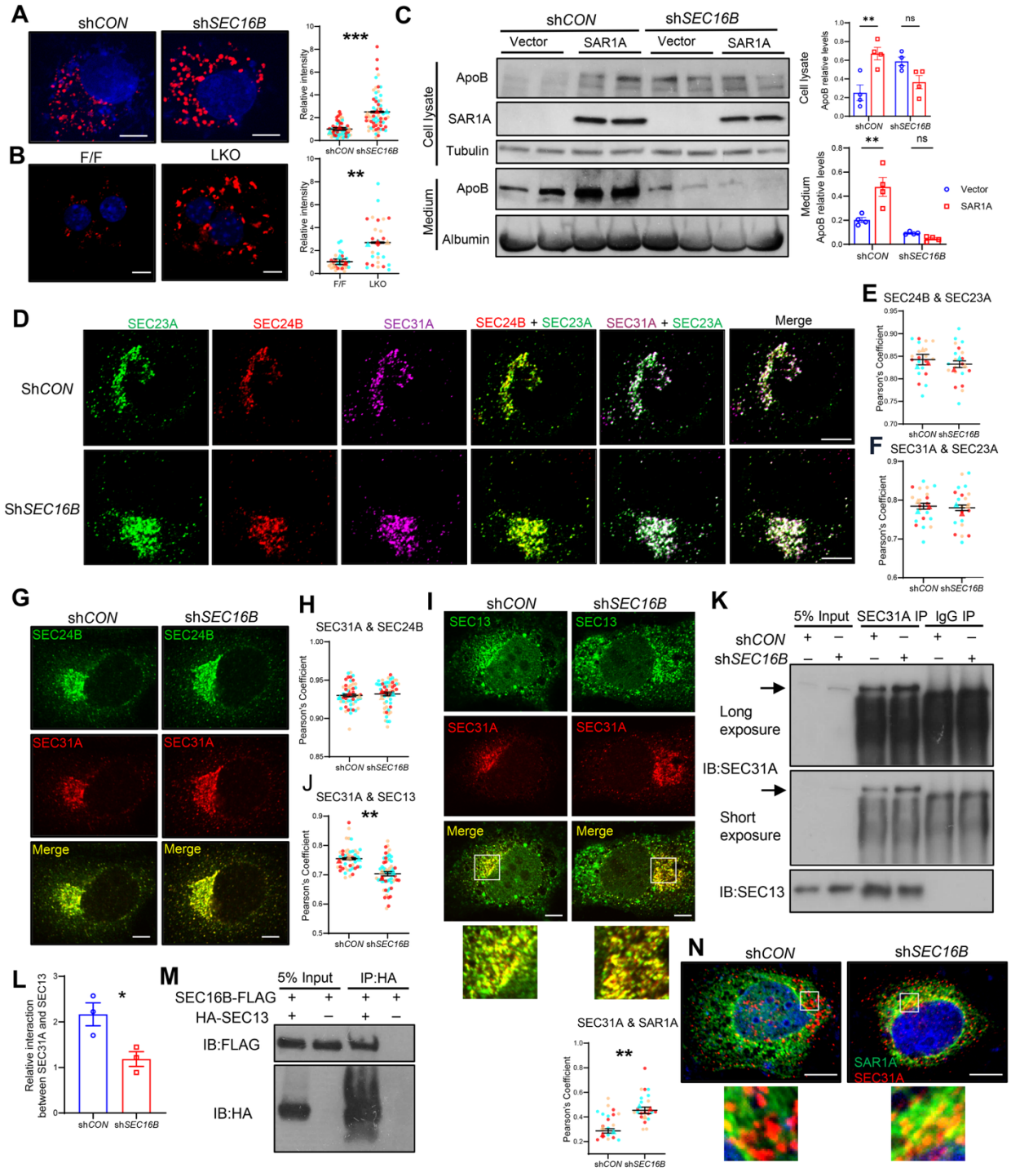


**Figure 4: SEC16B modulates the interaction between SEC13 and SEC31A, thereby promoting ApoB secretion.**

**(A)** Immunostaining and quantification of relative intensity of SAR1-GTP (red) in sh*CON* and sh*SEC16B* Huh7 cells cultured in DMEM+OA for 6 h. Scale bar = 8 μm.

**(B)** Immunostaining and quantification of relative intensity of SAR1-GTP (red) in F/F and LKO primary hepatocytes cultured in maintenance medium. Scale bar = 8 μm.

**(C)** Representative western blot images and quantification of ApoB levels in the cell lysate and medium of sh*CON* and sh*SEC16B* Huh7 cells cultured in DMEM+OA for 16 h. Cells were transfected with vector control or SAR1A-HA (n=4).

**(D-F)** Colocalization (D) and Pearson's coefficients (E-F) of endogenous SEC31A (purple), SEC24B (red) and exogenous SEC23A (green) in sh*CON* and sh*SEC16B* Huh7 cells transfected with eGFP-SEC23A and cultured in DMEM+OA for 6 h (n=3). Scale bar = 8 μm.

**(G-H)** Colocalization (G) and Pearson's coefficients (H) of endogenous SEC24B (green) and SEC31A (red) in sh*CON* and sh*SEC16B* Huh7 cells cultured in DMEM+OA for 6 h (n=3). Scale bar = 8 μm.

**(I-J)** Colocalization (I) and Pearson's coefficients (J) of endogenous SEC13 (green) and SEC31A (red) in sh*CON* and sh*SEC16B* Huh7 cells cultured in DMEM+OA for 6 h (n=3). Scale bar = 8 μm.

**(K-L)** Co-IP (K) and quantification (L) of SEC31A interaction with SEC13 in sh*CON* and sh*SEC16B* Huh7 cells cultured in DMEM+OA for 6 h. The relative interaction levels between SEC31A and SEC13 were determined by normalizing the SEC13 signal to the SEC31A signal within the immunocomplex (n=3).

**(M)** SEC16B-FLAG and HA-SEC13 co-immunoprecipitation (Co-IP) assay in HEK293T cells (n=3).

**(N)** Colocalization and Pearson's coefficients of exogenous SAR1A (green) and endogenous SEC31A (red) in sh*CON* and sh*SEC16B* Huh7 cells transfected with SAR1A-HA and cultured in DMEM+OA for 6 h (n=3). Scale bar = 8 μm.

Values are means ± SEM or violin plot. Statistical analysis was performed with two-way ANOVA (C), Student's t test (A, B, E, F, H, J, L and N). *P < 0.05, ***P < 0.001, ****P < 0.0001.

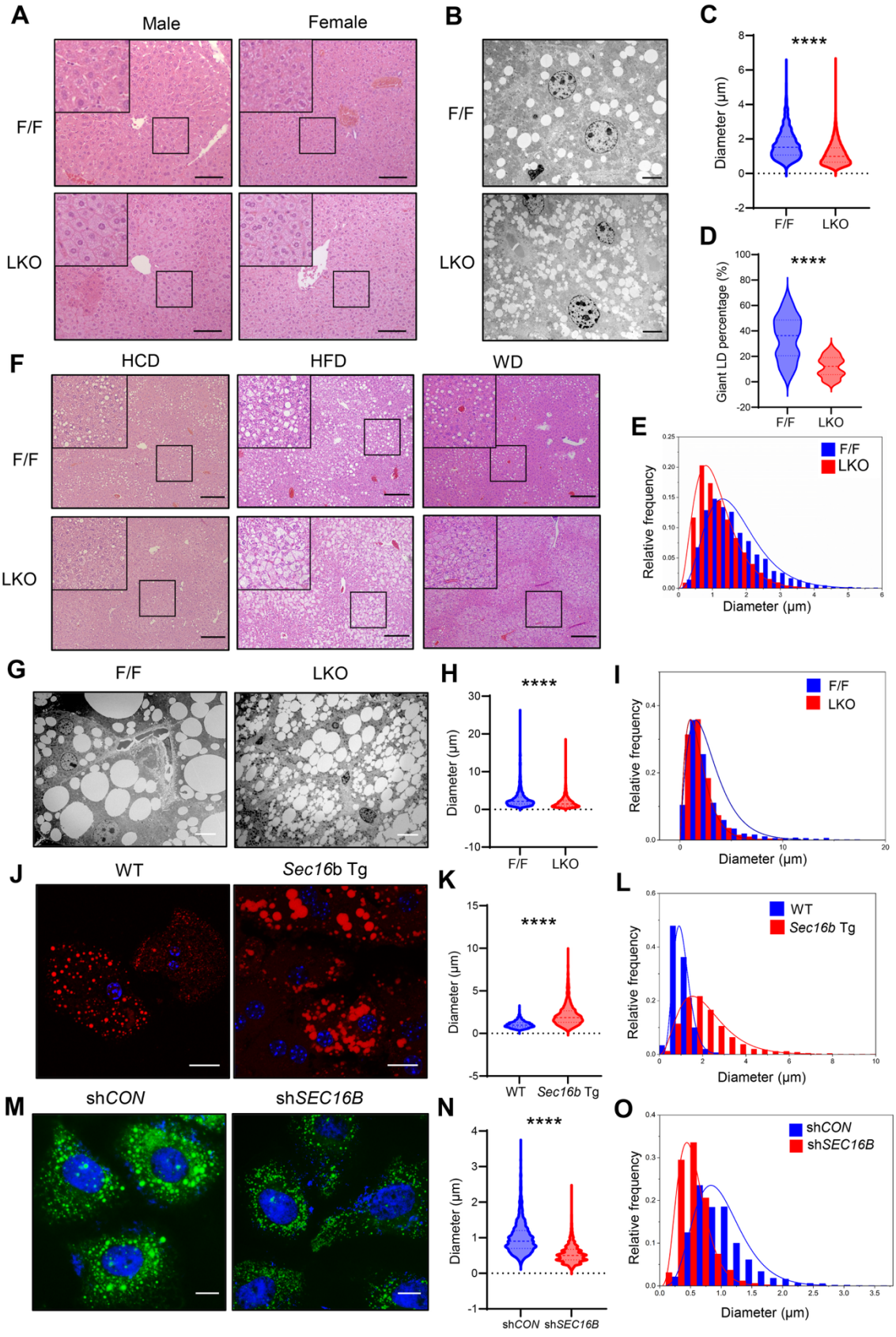
A
Male
Female
F/F
LKO
B
F/F
LKO
C
****
Diameter (μm)
F/F
LKO
D
****
Giant LD percentage (%)
F/F
LKO
E
F/F
LKO
Relative frequency
Diameter (μm)
F
HCD
HFD
WD
F/F
LKO
G
F/F
LKO
H
****
Diameter (μm)
F/F
LKO
I
F/F
LKO
Relative frequency
Diameter (μm)
J
WT
Sec16b Tg
K
****
Diameter (μm)
WT
Sec16b Tg
L
WT
Sec16b Tg
Relative frequency
Diameter (μm)
M
shCON
shSEC16B
N
****
Diameter (μm)
shCON
shSEC16B
O
shCON
shSEC16B
Relative frequency
Diameter (μm)

**Figure 5: SEC16B controls LD expansion in the liver.**

**(A)** Representative H&E staining of livers from control (F/F) and LKO mice fasted for 16 h (n=4). Scale bar = 100 μm.

**(B-C)** Representative electron microscopy (EM) images and quantification of LD diameter in the livers of male control (F/F) and LKO mice fasted for 16 h (n=3). Scale bar = 6 μm.

**(D-E)** Percentage of giant LD (diameter>2 μm) and the relative frequency of LD size in the livers of male control (F/F) and LKO mice fasted for 16 h.

**(F)** Representative H&E staining of livers from 8 weeks old male control (F/F) and LKO mice fed a high fat diet (HFD), high carbohydrate diet (HCD) and Western diet (WD) for 6-12 weeks (n=3). Scale bar = 200 μm.

**(G-I)** Representative EM images, quantification and relative frequency of LD size in the livers of WD-fed male control (F/F) and LKO mice (n=3). Scale bar = 8 μm.

**(J-L)** Representative images, quantification and relative frequency of LD size in male WT and *Sec16b* transgenic (Tg) primary hepatocytes treated with 200 μM OA (n=3). Scale bar = 20 μm.

**(M-O)** Representative images, quantification and relative frequency of LD size in sh*CON* and sh*SEC16B* Huh7 cells treated with 200 μM OA (n=3). Scale bar = 10 μm.

Values are means ± SEM or violin plot. Statistical analysis was performed with Student's t test (D) or Mann-Whitney test (C, H, K and N). ****P < 0.0001.

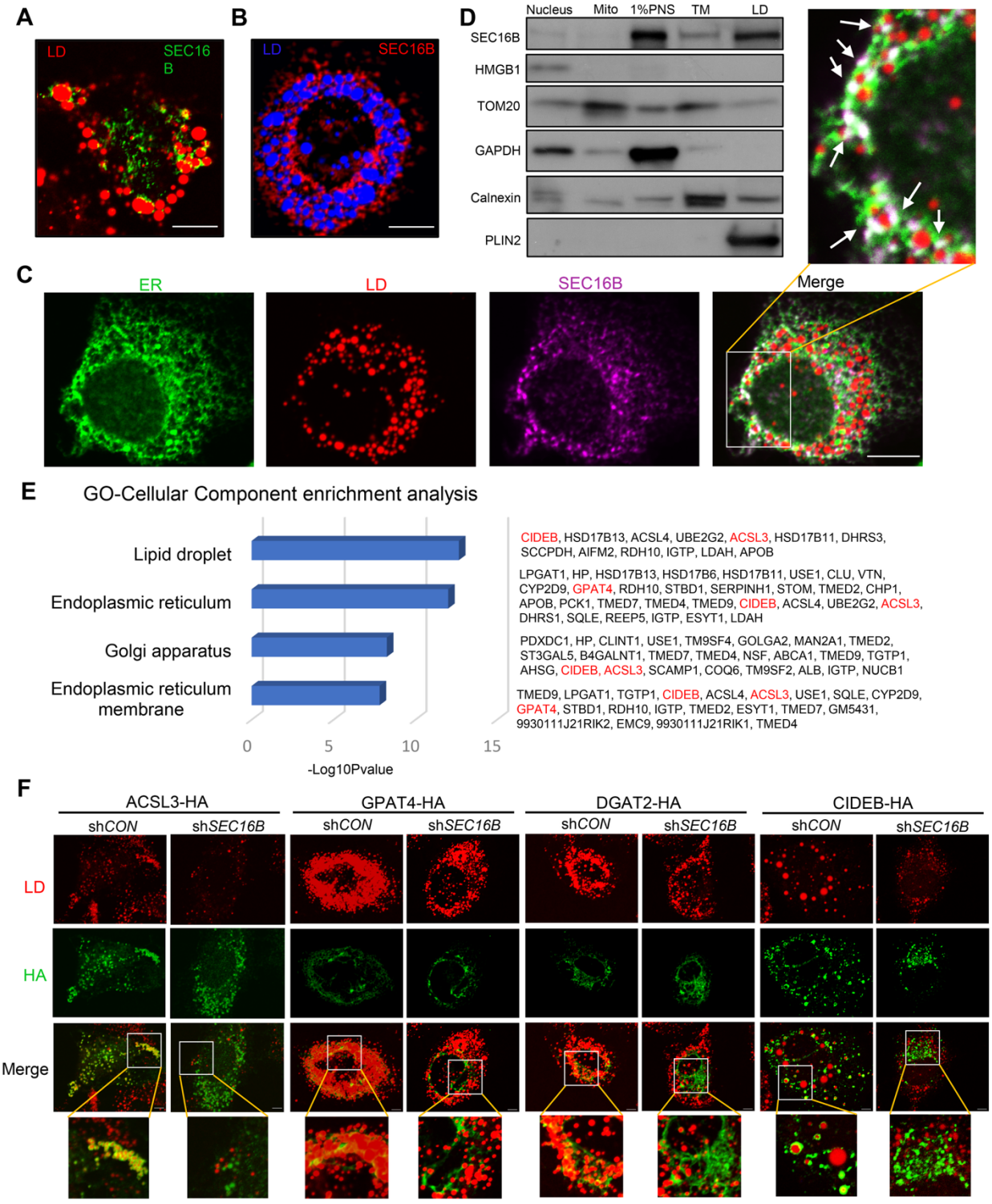


**Figure 6: SEC16B localizes to ER-LD contact sites and controls protein targeting to LDs.**

**(A)** Confocal microscope image of 6 h OA-treated Huh7 cells transfected with SEC16B-FLAG (green) and co-stained with LDs (red) (n=3).

**(B)** Confocal microscope image of 16 h OA-treated Huh7 cells transfected with SEC16B-FLAG (red) and co-stained with LDs (blue) (n=3).

**(C)** Confocal microscope image of 6 h OA-treated Huh7 cells transfected with SEC16B-FLAG (purple) and co-stained with LDs (red) and KDEL (green) (n=3).

**(D)** Western blot analysis of subcellular fractions from the livers of *Sec16b-3XFLAG*-transgenic male mice.

**(E)** Gene Ontology-Cellular Component enrichment analysis of downregulated proteins on LDs from male LKO mice compared to controls. Proteins labeled in red have been reported to localize to both ER and LDs and are associated with LD size (n=4-6).

**(F)** Confocal microscope analysis of 6 h OA-treated sh*CON* and sh*SEC16B* Huh7 cells transfected with HA-tagged ACSL3, GPAT4, DGAT2 and CIDEB (green) and co-stained with LDs (red) (n=3).

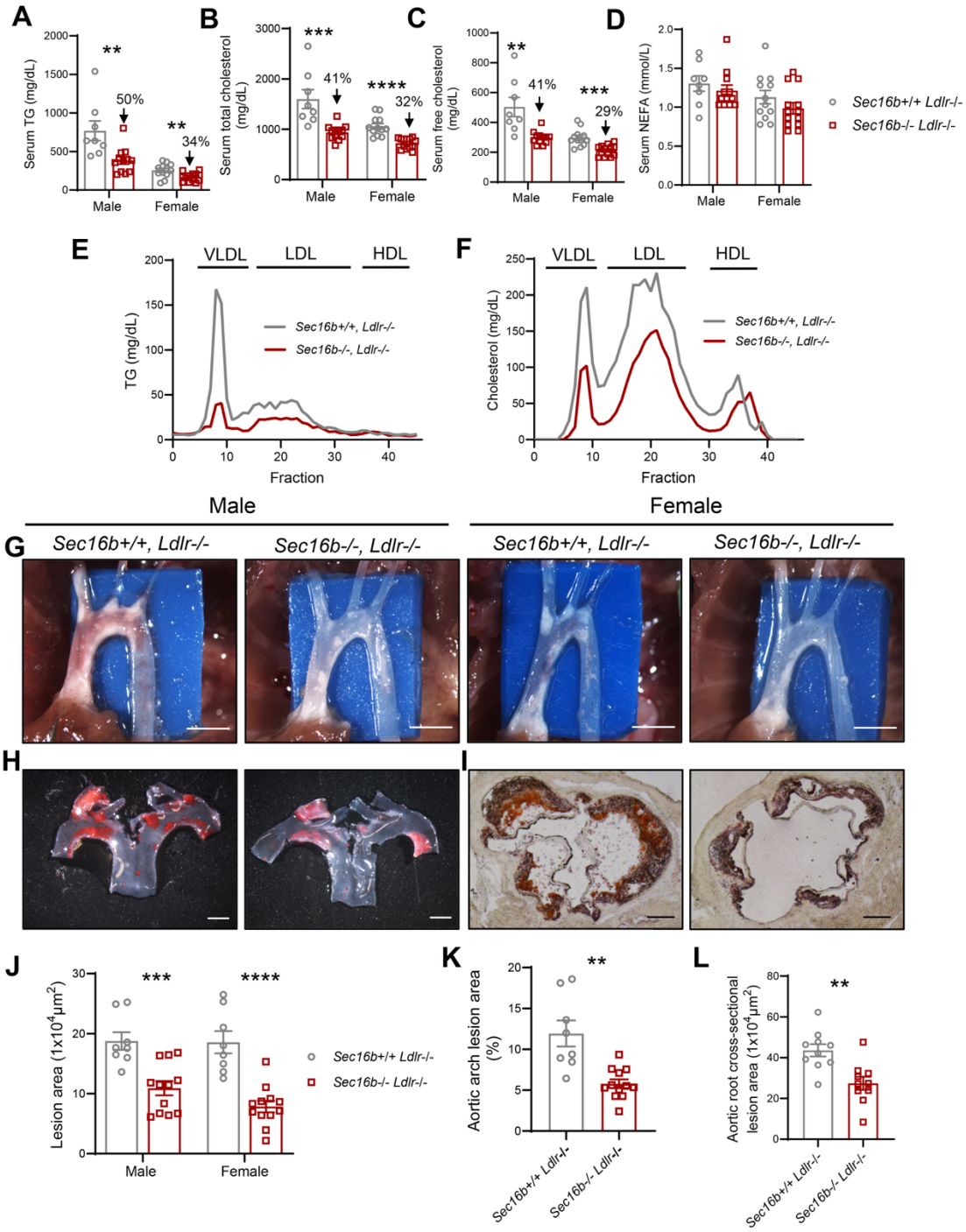


**Figure 7: Whole body *Sec16b* knockout protects against hyperlipidemia and atherosclerosis in *Ldlr* null mice.**

**(A-D)** Serum lipid levels of 8 weeks old *Sec16b+/+ Ldlr-/-* and *Sec16b-/- Ldlr-/-* mice fed WD for 12 weeks (n=8-13).

**(E-F)** FPLC analysis of lipoprotein profiles of serum from 8 weeks old male *Sec16b*+/+ *Ldlr-/-* and *Sec16b-/- Ldlr-/-* mice fed WD for 12 weeks. Serum from 7 mice/group was pooled.

**(G-I)** Representative images of aorta (G), *en face* aortic arch (H), and aortic root section (I) from 8 weeks old *Sec16b*+/+ *Ldlr-/-* and *Sec16b-/- Ldlr-/-* mice fed WD for 12 weeks (G-H: n=8-12, I: n=10). Scale bar = 1 mm (G-H) and 200 μm (I).

**(J-L)** Quantifications of aortic lesion areas in G-I.

Values are means ± SEM. Statistical analysis was performed with Student's t test. **P < 0.01, ***P < 0.001, ****P < 0.0001.

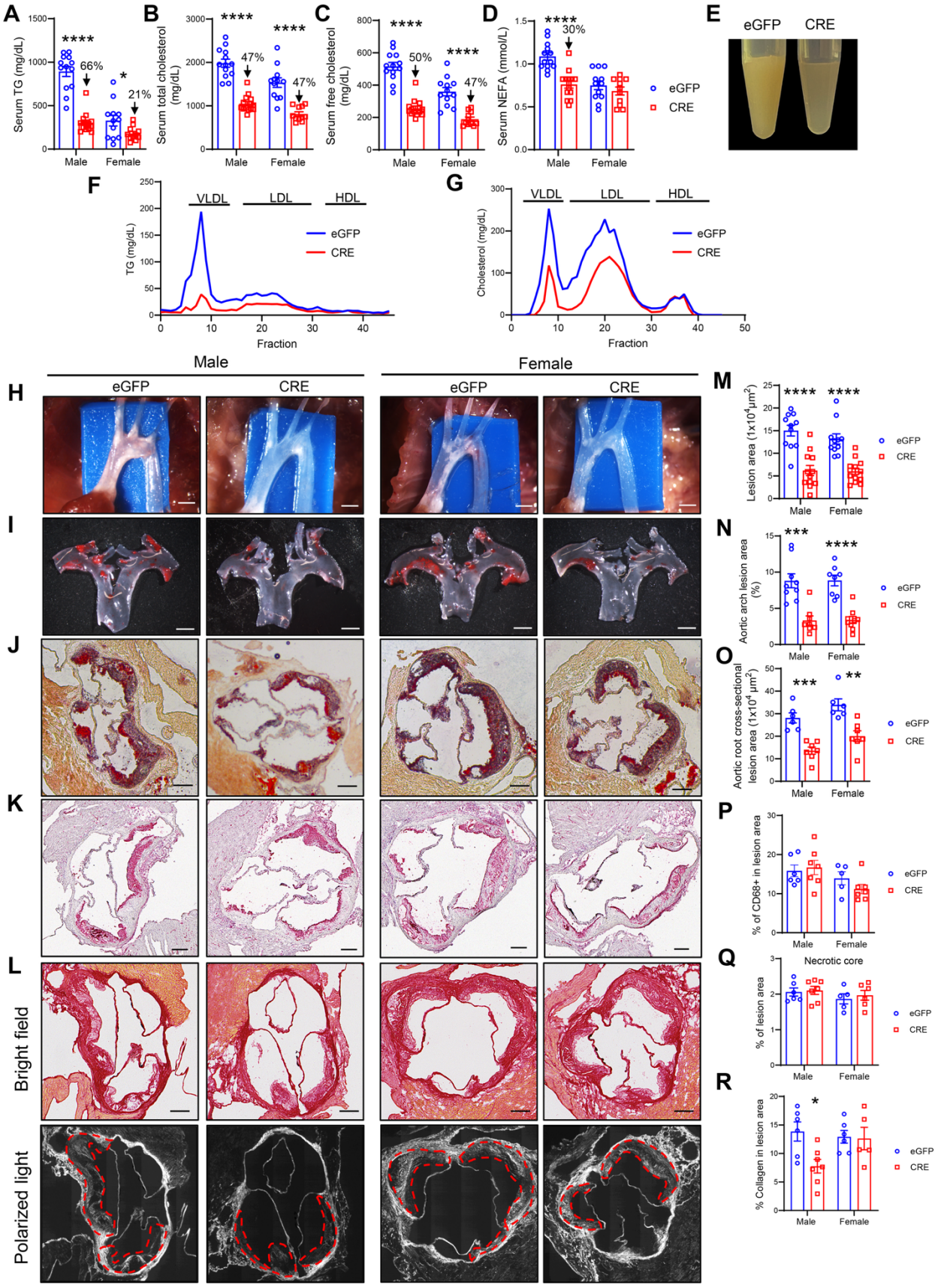
A
Serum TG (mg/dL)
****
66%
*
21%
Male
Female
B
Serum total cholesterol (mg/dL)
****
47%
****
47%
C
Serum free cholesterol (mg/dL)
****
50%
****
47%
D
Serum NEFA (mmol/L)
****
30%
eGFP
CRE
E
eGFP
CRE
F
TG (mg/dL)
VLDL
LDL
HDL
eGFP
CRE
Fraction
G
Cholesterol (mg/dL)
VLDL
LDL
HDL
eGFP
CRE
Fraction
Male
Female
eGFP
CRE
H
I
J
K
L
Bright field
Polarized light
M
Lesion area (1x10⁴ µm²)
****
****
N
Aortic arch lesion area (%)
***
****
O
Aortic root cross-sectional lesion area (1x10⁴ µm²)
***
**
P
% of CD68+ in lesion area
Q
Necrotic core
% of lesion area
R
% Collagen in lesion area
*

**Figure 8: Hepatic *Sec16b* deficiency ameliorates hyperlipidemia and atherosclerosis in *Ldlr* null mice.**

**(A-D)** Serum lipid levels in 12-week WD-fed *Sec16b*$^{F/F}$(F/F) *Ldlr*-/- mice receiving eGFP or CRE AAV (n=11-14).

**(E)** Gross image of serum from 12-week WD-fed male *Sec16b*$^{F/F}$(F/F) *Ldlr*-/- mice receiving eGFP or CRE AAV.

**(F-G)** FPLC analysis of lipoprotein profiles in serum from 12-weeks WD-fed male *Sec16b*$^{F/F}$(F/F) *Ldlr*-/- mice receiving eGFP and CRE AAV. Serum from 7 mice/group was pooled.

**(H-J)** Representative images of aorta (H), *en face* aortic arch (I), aortic root section (J) from 12-week WD-fed *Sec16b*$^{F/F}$(F/F) *Ldlr*-/- mice receiving eGFP or CRE AAV (H: n=11-13, I: n=8-9, J: n=6-7,). Scale bar = 1 mm (H-I) and 200 μm (J).

**(K-L)** Representative images of CD68 immunostaining (K) and Sirius red staining (L) of aortic root section from 12-week WD-fed *Sec16b*$^{F/F}$(F/F) *Ldlr*-/- mice receiving eGFP or CRE AAV (n=5-7). Scale bar = 200 μm.

**(M-R)** Quantification of aortic lesion areas in H-J, and percentage of CD68+ macrophage, necrotic core area and collagen content in aortic root lesions in K-L.

Values are means ± SEM. Statistical analysis was performed with Student's t test. *P < 0.05, **P < 0.01, ***P < 0.001, ****P < 0.0001.